



Universitat Ramon Llull

TESI DOCTORAL

Títol	Design and development of biomimetic surfaces and three-dimensional environments to study cell behavior
Realitzada per	Núria Mari Buyé
en el Centre	Escola Tècnica Superior IQS
i en el Departament	Bioenginyeria
Dirigida per	Dr. Salvador Borrós i Dr. Carlos E. Semino

Als pares

*Human subtlety will never devise an invention
more beautiful, more simple or more direct than does nature
because in her inventions nothing is lacking, and nothing is superfluous.*

Leonardo Da Vinci (1452-1519)

*La subtileza humana mai podrà concebre una invenció
més bella, més simple o més directa que la Naturalesa
perquè, en les invencions d'aquesta, res hi falta, res hi és superflu.*

Leonardo Da Vinci (1452-1519)

ACKNOWLEDGEMENTS

Escriure les primeres paraules d'aquesta pàgina és senyal d'estar ja al final... al final d'una tesi i al final de tota una etapa. És molta la gent a qui he d'agrair oportunitats, ajuda, saviesa, paciència, diversió, companyonia i aquells copets a l'esquena que de vegades fan tanta falta. La gent que em coneix bé sap que no em caracteritzo pas per tenir una bona memòria, així que a tots aquells que m'han envoltat durant aquests anys, moltes gràcies.

Dit això, agrair als meus directors de tesi al Prof. Salvador Borrós i al Prof. Carlos Semino per la grandiosa oportunitat d'acollir-me en els seus grups i per crear-me un projecte a mida, que amb molta flexibilitat hem anat adaptant al llarg dels anys. Gràcies per aquell toc de motivació diària i per confiar en mi per fer les estades al MIT i al TRM. Chicho, moltes gràcies per incloure'm en la gran família de Materials, per molts i molts consells i per ajudar-me a créixer professionalment i com a persona. *Carlos, gracias por introducirme al complejo mundo de la célula y de las "hamburguesas" (las celulares y las del O'Sullivan), por ser una constante fuente de ideas y por compartirlas conmigo. Por la confianza depositada en mi en tantas ocasiones.*

I am very grateful to Prof. Karen K. Gleason, who gave me the challenging opportunity to work in her lab at MIT for 6 months. Not only was I taught in numerous new techniques, but also the experience was a golden chance for my research and future career. Thanks to all the guys working at the g-lab at that time: Malancha, Sal, Long Hua, Wyatt, Taylor, Sung Gap and especially Shannan, who introduced me first to the iCVD world.

Thank you also to all the people at the Translationzentrum für Regenerative Medizin (TRM) in Leipzig who welcomed me to the institution as one of its first students. I truly appreciate the support from Matthias Braun, Hans Jörg Meisel and also from all the administration people. Moreover, I want to thank all the work that Bianca, Sven and the other people of the Semino's group did at TRM after I left. Thanks Bianca for your invaluable help!

Agradecer también al Dr. Jesús Otero del Hospital Universitario Central de Asturias en Oviedo por su colaboración y por proporcionarnos los fibroblastos humanos. A Ana Sancho y Elena de Juan-Pardo del CEIT y TECNUN (Universidad de Navarra) por los análisis de FEG-SEM. A la Plataforma Nanotecnológica de Barcelona, a Judith Linacero por su ayuda con la deshidratación de nuestras muestras y con el SEM, a Álvaro Mata por echarme siempre una mano y por su contribución en muchos proyectos, y a Esther por ser una muy buena compañera (gracias por el apoyo en la charla de TERMIS!). Agrair a la Carol Soler de l'IGTP per les crioseccions de les "hamburgueses".

També vull expressar la meva gratitud a molta gent de la casa. Al Carles Colominas, qui em va guiar en els meus primers passos en el món de la investigació i em va ensenyar algunes coses que encara tinc ben presents. També a la Núria Agulló, que és un puntal al Laboratori de Materials, i que sempre s'ha mostrat disposada a donar un cop de mà. A la Monte Agut que em va deixar les seves instal·lacions per alguns experiments quan nosaltres no teníem ni incubadors i sobretot per proporcionar-me un lloc tranquil per poder redactar durant aquests últims mesos. També agrair al Laboratori d'espectrofotomètrics per donar-me accés a l'espectrofotòmetre d'absorció atòmica i al Jordi Abellà pels anàlisi de SEM-EDS.

Moltes gràcies als veïns bio-frikis, que sempre han tingut la porta oberta per qualsevol cosa que he necessitat. Gràcies a la Magda, a en Joan, al Trevor, a la Neus, la Núria i a molts d'altres! *Y a Edu y a Javi, por contribuir además a noches apoteósicas.* Gràcies a l'Òscar de Micro, per la perfecta combinació de silenci i companyia en l'etapa de redacció. Ha estat realment un plaer també compartir tots aquests anys de doctorat amb els antics cimatencs i cimatencs i amb tota la gent nova del Biosotano. És tanta la gent que ha passat pel Laboratori de

Materials que difícilment em podria recordar de tots! Molt especialment gràcies al Jose, amb qui hem compartit molts i molts anys ja des de la carrera. Al trio la-la-la: la Laura, la Maria i l'Anna. Als més nous que han viscut amb mi aquests últims anys: a la Nathaly, al Pri, al Greg, als meus nens en Joan i l'Ana, a l'Òscar, a la Djamila. I al Víctor, moltíssimes gràcies pels consells! Gràcies a tots i cadascun de vosaltres pel recolzament diari i per fer el dia a dia més divertit. Un agraïment molt i molt especial a totes les meves nenes teixidores. Ha estat un autèntic plaer treballar amb totes vosaltres i he de dir que em sento molt orgullosa de veure com, gràcies a la feina de cadascuna, aquest laboratori ha anat canviant a millor, cada vegada més professional i més ben organitzat! Gràcies Tere, Cris, Mireia, Vero, Patri, Lourdes, Caterina, Irene i a la Desi, que sempre la considerarem una més de grup! Aquesta última etapa no hagués sigut el mateix sense vosaltres!

A l'IQS he tingut la sort de conèixer molta altra gent increïble, començant per la Núria, qui ha passat de ser la companya d'informes absolutament perfecte a ser una gran amiga. Gràcies per tots els moments viscuts, pels antics dinars al Químic que ara ja ens queden tan lluny i encara més per haver convertit això en tants altres moments fora de l'IQS (que així segueixi). Gràcies a la Berta, per ser insistent i exigir-me, per ser-hi sempre que et necessito *no matter where you are* i per una època totalment incomparable! *A Vane i a Ana, por tantos buenos momentos compartidos dentro y fuera del IQS.* Al Xavi, amb qui sempre hem estat molt units des que ens barallàvem amb els VAPs i VEPs a primer. *A Andrea, por las confiancias y muchísimas risas; el IQS ya no fue lo mismo sin ti!* A la Cris, pels vinillos i les llargues converses (ho trobaré molt a faltar). A fora de l'IQS, mil gràcies a la meva Marta, perquè sempre hi ets! Als amics de Sant Andreu i de Sa Cala, per l'esforç d'entendre el que ha estat la meva passió durant aquests anys.

Gracias a una botella de vinagre de Módena Borges, a un vuelo de Ryanair y a la ciudad de Sevilla, que unidos bajo un cúmulo de casualidades impensables me llevaron a conocer a una de las personas que más intensamente ha compartido mis últimos años de esta etapa. Gracias David por tu influjo de energía, creatividad, positividad e incondicional confianza en mí.

Finalment, gràcies a tota la meva família, la d'aquí i la d'Eivissa. Gràcies als avis, que cada dia em demostren que estan orgullosos de mi. I a es güelos, que sé que també ho estan allà on siguin. Gràcies a l'Albert, a qui admiro i amb qui sempre puc comptar, sigui on sigui. També a l'Ana, que és un sol. I molt especialment, gràcies als pares, que són el meu model i exemple en molts sentits, i que en definitiva són els que viuen amb més entusiasme els meus èxits, però també amb més preocupació les meves frustracions. Els hauria d'agrair tantes coses que no acabaria mai i és per això vull dedicar-los aquest treball.

Núria
22 d'abril de 2012

This thesis has been possible thanks to a predoctoral FI fellowship (2006 FI 00447) and mobility BE grant (2006 BE 00526) from DURSI (Generalitat de Catalunya) and the European Social Fund and to the Translational Centre for Regenerative Medicine, Leipzig University (Germany), Award 1098 NF, as well as to the Institut Químic de Sarrià.

SUMMARY

Biomimetics or biomimicry are terms that imply “learning from nature”, from its systems, processes and models, in order to use nature as inspiration to solve human problems. In tissue engineering, biomimetics is nowadays a recurrent term and a source of ideas to obtain more elegant and sophisticated platforms that could better mimic the interactions between cells and their environment. This thesis is focused on developing models both in two- and three-dimensions by recreation of one or more factors of the cell natural environment that are known to play an important role in cell behavior.

Since both the chemical and mechanical properties of the extracellular matrix are known to effectively influence cell function, an innovative polymeric thin film was designed combining a hydrogel with tunable mechanical properties and a reactive molecule, capable to immobilize biomolecules. Due to the complexity of the polymers, a versatile technique such as initiated chemical vapor deposition (iCVD) was required for the synthesis. Extensive characterization revealed that nanostructured hydrogels were obtained and that small biomolecules, such as signaling peptides, could be attached on the surface. The final surfaces are bioactive and support endothelial cell attachment.

Relevant biomimetic surfaces for bone tissue engineering could also be obtained from a sol-gel synthesized hydroxyapatite after immersion in different physiological media. The dissolution and posterior reprecipitation of the ions rendered a final apatite layer with a composition similar to that found *in vivo*. The experiments evidenced the importance of starting from a rather soluble material and, thus, pure hydroxyapatite was not able to promote apatite precipitation *in vitro*. This capacity has been related to the material bioactivity by many researchers in terms of its ability to bond to bone in tissue engineering applications.

However, for tissue engineering a three-dimensional environment is required to build tissue-like constructs. A new model was developed based on the use of a very soft gel to obtain hard tissue. Although the concepts might seem to work in opposite directions, cells gain the ability to rapidly elongate and form a dense cellular network within this unrestrictive environment. Subsequent contraction of the whole system rendered a smaller and stronger final tissue-like construct. This system was considered biomimetic as it promotes high cell-cell interaction and cellular condensation, which are events that occur in bone and cartilage development. This system was extensively characterized with osteoprogenitor MC3T3-E1 cells that could undergo full osteogenic differentiation under chemical induction. More interestingly, the three-dimensional microenvironment was also able to promote by itself spontaneous expression of bone-related markers. Due to the interesting properties of this system, the same model was used to induce chondrogenic differentiation of human dermal fibroblasts. This cell type has been poorly explored for tissue engineering applications, but it might have great potential in future therapeutic platforms. This work provides proof of concept of chondrogenic potential of these cells in this three-dimensional system.

RESUM

La biomimètica o biomimetisme són termes que simbolitzen el concepte “aprendre de la naturalesa”, és a dir, aprendre dels seus sistemes, processos i models, a fi d'utilitzar la natura com a font d'inspiració per solucionar problemes de l'home. El biomimetisme és actualment un concepte recurrent en l'àrea d'enginyeria de teixits i d'ell en sorgeixen idees per obtenir plataformes més elegants i sofisticades que puguin imitar millor les interaccions entre les cèl·lules i el seu ambient. Aquesta tesi pretén desenvolupar models, en dues i en tres dimensions, mitjançant la recreació d'un o més factors característics de l'ambient natural de la cèl·lula i que juguen un paper important en el comportament cel·lular.

Se sap que tant les propietats químiques com les mecàniques de la matriu extracel·lular influeixen sobre les funcions cel·lulars. És per això que es va dissenyar un nou film polimèric que pogués combinar un hidrogel, amb propietats mecàniques variables, amb un monòmer reactiu capaç d'immobilitzar biomolècules. Degut a la complexitat del polímer dissenyat, va ser necessari recórrer a una tècnica de polimerització superficial molt versàtil com és la deposició química iniciada en fase vapor (més coneguda pel seu acrònim en anglès iCVD). Els polímers varen ser àmpliament caracteritzats i es va corroborar que podien ser modificats amb petites biomolècules com ara pèptids senyalitzadors. Les superfícies resultants són bioactives i permeten l'adhesió de cèl·lules endotelials.

Unes altres superfícies biomimètiques, rellevants en l'àmbit de l'enginyeria de teixits d'os, es varen obtenir a partir d'una hidroxiapatita sintetitzada pel mètode de sol-gel submergint-la en diferents medis fisiològics. La dissolució i posterior reprecipitació dels ions proporcionen una capa d'apatita amb una composició similar a la que es troba *in vivo*. Els experiments evidencien la importància de partir d'un material relativament soluble. És per això que la hidroxiapatita pura no és capaç d'induir la precipitació d'aquesta apatita biomimètica *in vitro*. Diversos investigadors han relacionat la capacitat de formar apatita amb la bioactivitat del material, entenent bioactivitat com l'habilitat d'aquests materials de promoure la unió amb l'os.

Per a l'enginyeria de teixits, però, és necessari un ambient tridimensional per tal de generar un teixit artificial. S'ha desenvolupat un nou model basat en l'ús d'un gel molt tou per tal d'obtenir un teixit dur com el de l'os. Malgrat que aquests dos conceptes poden semblar contradictoris, les cèl·lules adquireixen l'habilitat d'allargar-se ràpidament i crear una densa xarxa cel·lular dins d'aquest ambient poc restrictiu des d'un punt de vista mecànic. La consegüent contracció del sistema acaba formant un constructe més petit i resistent. Aquest és un sistema biomimètic ja que promou una gran interacció cel·lular i també la condensació de les cèl·lules, esdeveniments que tenen lloc també durant el desenvolupament de l'os i el cartílag. El model es va caracteritzar extensament amb cèl·lules ostoprogenitores MC3T3-E1 que es diferenciaren amb inducció química. A més a més, es va demostrar que l'ambient tridimensional podia promoure l'expressió espontània de marcadors osteogènics. Degut a les interessants propietats del sistema, el mateix model es va utilitzar per induir la diferenciació condrogènica de fibroblastos dermals humans. Aquests tipus cel·lular no ha estat gaire explorat en l'àmbit de l'enginyeria de teixits, malgrat que ofereix un gran potencial en teràpia regenerativa. Aquest treball proporciona proves de la capacitat condrogènica d'aquestes cèl·lules en el sistema tridimensional prèviament desenvolupat.

RESUMEN

La biomimética o biomimetismo son términos que simbolizan el concepto “aprender de la naturaleza”, es decir, aprender de sus sistemas, procesos y modelos, y utilizarlos como fuente de inspiración para solucionar problemas del hombre. El biomimetismo es actualmente un concepto recurrente en el área de ingeniería de tejidos y de este surgen ideas para obtener plataformas más elegantes y sofisticadas que puedan mimetizar mejor las interacciones entre las células y su ambiente. La presente tesis se centra en desarrollar modelos, tanto en dos como en tres dimensiones, mediante la recreación de uno o más factores que caracterizan el ambiente natural de la célula y que tienen su rol importante en el comportamiento celular.

Se conoce que tanto las propiedades químicas como mecánicas de la matriz extracelular influyen en las funciones celulares. Debido a esto, se diseñó un nuevo film polimérico que pudiera combinar un hidrogel, con propiedades mecánicas variables, con un monómero reactivo, capaz de inmovilizar biomoléculas. Debido a la complejidad del polímero diseñado, fue necesario recurrir a una técnica de polimerización superficial muy versátil como es la deposición química iniciada en fase vapor (más conocida por su acrónimo en inglés iCVD). Los polímeros fueron ampliamente caracterizados y se corroboró que podían ser modificados con pequeñas biomoléculas como péptidos señalizadores. Las superficies resultantes son bioactivas y permiten la adhesión de células endoteliales.

Se obtuvieron otro tipo de superficies biomiméticas relevantes en el ámbito de la ingeniería de tejidos de hueso, a partir de una hidroxiapatita sintetizada por el método sol-gel sumergiéndolas en diferentes medios fisiológicos. La disolución y posterior reprecipitación de los iones proporcionan una capa de apatita con una composición similar a la que se encuentra *in vivo*. Los experimentos evidencian la importancia de partir de un material relativamente soluble. Precisamente debido a esto la hidroxiapatita pura no es capaz de inducir la precipitación de esta apatita biomimética *in vitro*. Varios investigadores han relacionado la capacidad de formar apatita con la bioactividad del material, entendiendo bioactividad como la habilidad de estos materiales de promover la unión con el hueso.

De todos modos, en ingeniería de tejidos, es necesario un ambiente tridimensional para generar un tejido artificial. Se ha desarrollado un nuevo modelo basado en el uso de un gel blando para obtener tejido duro como el del hueso. Aunque estos conceptos pueden parecer contradictorios, las células adquieren la habilidad de estirarse rápidamente y de formar una densa red celular dentro de este gel tan poco restrictivo desde un punto de vista mecánico. La consiguiente contracción del sistema acaba formando un constructo mucho más pequeño y resistente. Este es un sistema biomimético ya que promueve una gran interacción celular y también la condensación de las células, eventos que también ocurren durante el desarrollo de hueso y cartílago. El modelo se caracterizó extensamente con células osteoprogenitoras MC3T3-E1 que se diferenciaron bajo inducción química. Además, se demostró que el microambiente tridimensional podía promover la expresión espontánea de marcadores osteogénicos. Debido a las interesantes propiedades del sistema, el mismo modelo se usó para inducir la diferenciación condrogénica de fibroblastos dermales humanos. Este tipo celular no ha sido demasiado explorado en ingeniería de tejidos, a pesar de que puede tener un gran potencial en terapia regenerativa. Este trabajo proporciona pruebas de la capacidad condrogénica de estas células en el sistema tridimensional previamente desarrollado.

TABLE OF CONTENTS

ACKNOWLEDGEMENTS	VII
SUMMARY	IX
RESUM	XI
RESUMEN	XIII
TABLE OF CONTENTS	XV
LIST OF FIGURES	XIX
LIST OF TABLES	XXIII
LIST OF ABBREVIATIONS	XXV
LIST OF PUBLICATIONS	XXVII
CHAPTER 1. INTRODUCTION TO CELL MICROENVIRONMENT AND BIOMIMETICS	1
1.1. <i>Background</i>	3
1.1.1. Biomimetics: learning from nature	3
1.1.2. An overview of the natural cell environment	4
1.1.3. Biomimetics in tissue engineering: deconstructing the complex biological environment into simple systems (models)	7
1.2. <i>Motivation and general aims</i>	10
1.3. <i>Content of this dissertation</i>	10
1.4. <i>References</i>	12
CHAPTER 2. BIOMIMETIC POLYMERIC THIN FILMS COMBINING BIOCHEMICAL AND BIOPHYSICAL PROPERTIES	15
2.1. <i>Background</i>	17
2.1.1. Overview	17
2.1.2. How cells sense the environment	17
2.1.3. Models mimicking chemical signaling	18
2.1.4. Impact of matrix physical properties on cell function	18
2.1.5. Models combining chemical and mechanical signaling	19
2.1.6. Single-step functionalization: pentafluorophenyl methacrylate	20
2.1.7. Initiated chemical vapor deposition (iCVD)	21
2.2. <i>Hypothesis and specific aims</i>	23
2.3. <i>Materials and methods</i>	23
2.3.1. iCVD polymerization	23
2.3.2. Sample reactivity	24
2.3.3. Surface characterization	25

2.3.4.	Biological assessment	27
2.4.	<i>Results and discussion</i>	28
2.4.1.	PFM polymerization	28
2.4.2.	PFM functionalization	33
2.4.3.	HEMA hydrogels with PFM	37
2.4.4.	Experiments to test biological behavior.....	50
2.5.	<i>Concluding remarks</i>	56
2.6.	<i>References</i>	58

CHAPTER 3. BIOMIMETIC APATITE LAYER ON SYNTHETIC HYDROXYAPATITE 63

3.1.	<i>Background</i>	65
3.1.1.	Overview	65
3.1.2.	Bone microenvironment: a mineralized hierarchical matrix	65
3.1.3.	Biom mineralization process.....	66
3.1.4.	Biomimetic strategy to produce apatite coatings.....	67
3.1.5.	Synthetic sol-gel hydroxyapatite.....	68
3.2.	<i>Hypothesis and specific aims</i>	69
3.3.	<i>Materials and methods</i>	69
3.3.1.	Sol-gel synthesis of hydroxyapatite	69
3.3.2.	Characterization of hydroxyapatite	70
3.3.3.	Hydroxyapatite interaction with physiological media	72
3.4.	<i>Results and discussion</i>	73
3.4.1.	Previous theoretical studies on the calcium phosphates precipitation in physiological media	73
3.4.2.	Interaction of the sol-gel synthesized hydroxyapatite with physiological media	78
3.4.3.	Morphology and elemental composition of the new layer on synthesized hydroxyapatite	84
3.5.	<i>Concluding remarks</i>	87
3.6.	<i>References</i>	89

CHAPTER 4. OSTEOGENIC DIFFERENTIATION IN 3D SOFT SELF-ASSEMBLING PEPTIDE 95

4.1.	<i>Background</i>	97
4.1.1.	Overview	97
4.1.2.	Basics of bone development: migration, communication, condensation and differentiation	97
4.1.3.	The third dimension: resembling the structure of the extracellular matrix	99
4.1.4.	Matrix stiffness influence in osteogenic differentiation: 2D vs 3D	100
4.1.5.	Cellular elongation, migration and cell-cell contact in hydrogels.....	101
4.2.	<i>Hypothesis and specific aims</i>	102
4.3.	<i>Materials and methods</i>	102
4.3.1.	Cell expansion	102
4.3.2.	Cell encapsulation in self-assembling peptide	103

4.3.3.	ROCK inhibitor assays	105
4.3.4.	Osteogenic differentiation.....	105
4.3.5.	Cell culture on self-assembling peptide hydrogel.....	105
4.3.6.	Cellular and construct morphology evaluation: phase contrast and fluorescence microscopy.....	106
4.3.7.	Field emission gun-scanning electron microscopy (FEG-SEM) analysis.....	106
4.3.8.	Cell viability assessment	107
4.3.9.	RNA isolation and quantitative reverse transcriptase polymerase chain reaction (qRT-PCR)	107
4.3.10.	Phenotype assessment by staining.....	108
4.3.11.	Preparation of cryosections.....	109
4.3.12.	Statistical analysis	109
4.4.	<i>Results and discussion</i>	110
4.4.1.	Morphological changes on the global construct.....	110
4.4.2.	Cellular behavior within the self-assembling peptide	113
4.4.3.	Osteogenic differentiation of pre-osteoblastic cells in 3D self-assembling peptide hydrogel	116
4.4.4.	Cell viability in the constructs.....	126
4.4.5.	MC3T3-E1 constructs under the influence of other medium supplements	128
4.5.	<i>Concluding remarks</i>	132
4.6.	<i>References</i>	134

CHAPTER 5. CHONDROGENIC POTENTIAL OF HUMAN DERMAL FIBROBLASTS IN SOFT SELF-ASSEMBLING PEPTIDE GEL..... 141

5.1.	<i>Background</i>	143
5.1.1.	Overview.....	143
5.1.2.	Cartilage formation and extracellular matrix components.....	143
5.1.3.	Cartilage tissue engineering.....	145
5.1.4.	Spontaneous chondrogenesis of mouse embryonic fibroblasts in self-assembling peptide gel	148
5.2.	<i>Hypothesis and specific aims</i>	148
5.3.	<i>Materials and methods</i>	149
5.3.1.	Cell expansion	149
5.3.2.	Cell encapsulation in 3D self-assembling peptide hydrogel	149
5.3.3.	Chondrogenic differentiation of 3D cultures	150
5.3.4.	Osteogenic differentiation of 3D cultures	150
5.3.5.	Cell viability assessment	150
5.3.6.	RNA and protein isolation from 2D and 3D cultures	150
5.3.7.	Quantitative reverse transcriptase polymerase chain reaction (qRT-PCR).....	151
5.3.8.	Western blot for collagen type II	152
5.3.9.	Glycosaminoglycans (GAGs) determination by toluidine blue staining.....	152
5.3.10.	Calcium deposits detection by von Kossa staining	153

5.4.	<i>Results and discussion</i>	153
5.4.1.	hNDF in self-assembling peptide gels: cellular network and system contraction	153
5.4.2.	Evaluation of spontaneous chondrogenic commitment in hNDF constructs	154
5.4.3.	Cell viability within the constructs	155
5.4.4.	Spontaneous calcification of dermal fibroblasts constructs	156
5.4.5.	Study of different supplements to induce chondrogenic differentiation	158
5.5.	<i>Concluding remarks</i>	162
5.6.	<i>References</i>	164
GENERAL PERSPECTIVE		169
CONCLUSIONS		171
APPENDICES		173
	<i>Appendix 1. Aminoacids symbol and structure</i>	173
	<i>Appendix 2. Flow and residence time calculation</i>	175
	<i>Appendix 3. RNA isolation and quantification</i>	176
	<i>Appendix 4. qRTPCR reaction preparation and calculations</i>	180
	<i>Appendix references</i>	184

LIST OF FIGURES

Figure 1.1.1-1. Comparison of Velcro structure with its natural analog, the burdock.	3
Figure 1.1.2-1. Microenvironmental factors affecting cell behavior.	4
Figure 1.1.2-2. Scheme of the basic ECM components in the 3D environment of the cells.	5
Figure 1.1.3-1. 2D versus 3D cultures.	9
Figure 2.1.2-1. Basic components of the focal adhesion complexes	18
Figure 2.1.6-1. Pentafluorophenyl methacrylate structure and reactivity.	20
Figure 2.1.7-1. iCVD reactor setup.	21
Figure 2.1.7-2. Reaction mechanism of a polymerization by iCVD.	22
Figure 2.3.1-1. Chemical structure of the monomers.	24
Figure 2.3.3-1. Angle-resolved XPS.	25
Figure 2.3.3-2. Dynamic contact angle scheme.	26
Figure 2.4.1-1. FTIR spectrum of PFM homopolymer film.	29
Figure 2.4.1-2. XPS high-resolution scan of the PFM homopolymer.	29
Figure 2.4.1-3. FTIR spectra of four polymer compositions.	32
Figure 2.4.2-1. Chemical structure of the amine-containing molecules used as control.	33
Figure 2.4.2-2. FTIR spectra of a crosslinked PFM film functionalization with diamine.	34
Figure 2.4.2-3. FTIR spectra of the diamine reaction with a crosslinked PFM film depending on the temperature.	35
Figure 2.4.2-4. XPS survey scan of the coupling of N-RYVVLPR-C peptide to PFM.	36
Figure 2.4.2-5. Immobilization of fluorescein-5-thiosemicarbazide.	37
Figure 2.4.3-1. FTIR spectra comparison showing the PFM incorporation into the hydrogel.	38
Figure 2.4.3-2. Crosslinking degree and swelling properties of HEMA-co-EGDA-co-PFM films.	39
Figure 2.4.3-3. Advancing and receding contact angle of the hydrogel with PFM before and after treated with diamine.	41
Figure 2.4.3-4. Scheme of the two approaches studied for the soft surfaces.	42
Figure 2.4.3-5. Contact angle measurements of the hydrogel / PFM films vs surface F / C ratio.	44
Figure 2.4.3-6. Schematic representation of the polymer brushes in different media.	45
Figure 2.4.3-7. Contact angle hysteresis of hydrogel / PFM and bare hydrogel films.	46
Figure 2.4.3-8. Decrease of the swelling ability in water for hydrogels with PFM on surface, compared to the bare hydrogels.	46
Figure 2.4.3-9. Swelling behavior of the two-layer hydrogels and the bare HEMA-co-EGDA.	47
Figure 2.4.3-10. Dynamic swelling studies.	48
Figure 2.4.3-11. AFM topographical micrographs of a hydrogel with a PFM layer on top.	49
Figure 2.4.4-1. Mouse embryonic fibroblasts morphology at 2 h of incubation.	51
Figure 2.4.4-2. Mouse embryonic fibroblasts morphology at 12 h of incubation.	51
Figure 2.4.4-3. Study of the cluster size of MEFs.	52
Figure 2.4.4-4. Scheme of the strategy to test the biological activity of the iCVD polymerized films.	53
Figure 2.4.4-5. HUVEC morphology at 2 h of incubation.	54
Figure 2.4.4-6. AFM micrographs of PFM and HEMA/PFM samples in water.	55

Figure 3.1.2-1. The structural hierarchy of compact bone.....	66
Figure 3.1.5-1. Schematic representation of the sol-gel route.....	69
Figure 3.3.1-1. Sol-gel synthesis of hydroxyapatite.	70
Figure 3.3.2-1. Standard diffraction pattern of hydroxyapatite	71
Figure 3.4.1-1. Free energy change for possible calcium phosphates and carbonate precipitates in SBF and α -MEM.....	75
Figure 3.4.1-2. Comparison of the thermodynamically and the kinetically favored phases as function of pH.....	77
Figure 3.4.2-1. Changing profile of the ionic composition and pH in SBF with the immersion of sHA.....	79
Figure 3.4.2-2. Composition changes in different media after sHA immersion.	80
Figure 3.3.2-3. Composition changes in media calcium or without phosphate.	81
Figure 3.4.2-4. Calcium release profile of commercial HA.	81
Figure 3.4.2-5. XRD spectra of synthetic and commercial hydroxyapatite.	82
Figure 3.3.2-6. XRD spectra of synthetic and commercial hydroxyapatite after immersion in physiological media.	83
Figure 3.4.3-1. SEM images of the new layer on the sol-gel synthesized hydroxyapatite.	84
Figure 3.4.3-2. Energy dispersive spectroscopy (EDS) of crystals grown in α -MEM.	86
Figure 3.4.3-3. Ca to P ratio variation with crystal size.	86
Figure 3.4.3-4. SEM images of the commercial hydroxyapatite soaked in media.	87
Figure 4.1.2-1. Bone formation via intramembranous and endochondral ossification.	98
Figure 4.1.2-2. Sequential stages in osteogenic differentiation.....	99
Figure 4.1.3-1. Self-assembling peptide RAD16-I.....	100
Figure 4.3.2-1. Schematic representation of the protocol for cell encapsulation in self-assembling peptide.	104
Figure 4.4.1-1. Morphological changes on MC3T3-E1 constructs over time.	111
Figure 4.4.1-2. Effect of self-assembling peptide concentration (or initial hydrogel stiffness) on the contraction process.....	111
Figure 4.4.1-3. FEG-SEM analysis of a contracted construct at final stage.	112
Figure 4.4.1-4. Compared morphology of the extracellular matrix in the construct and the original self-assembling peptide.	113
Figure 4.4.2-1. Cell morphology and cell network formation versus hydrogel stiffness.	114
Figure 4.4.2-2. Cellular network formation at the edge of a construct.	115
Figure 4.4.2-3. Role of ROCK in the regulation of actin fiber contractility and stabilization.	115
Figure 4.4.2-4. Effect of ROCK inhibitor on cell elongation and construct contraction.....	116
Figure 4.4.3-1. Mineralization of MC3T3-E1 progenitor cells in 2D and 3D cultures.....	117
Figure 4.4.3-2. Effect of dexamethasone (D) on mineralization of MC3T3-E1 cells in 2D and 3D cultures.....	118
Figure 4.4.3-3. Effect of dexamethasone time administration on mineralization.	120
Figure 4.4.3-4. Expression profile of osteogenic genes in encapsulated MC3T3-E1 cells cultured in different media.	120
Figure 4.4.3-5. Spontaneous expression of bone-related genes in 3D cultures of MC3T3-E1 cells.....	121
Figure 4.4.3-6. Bone-related protein expression in 3D and 2D cultures in the three media.	122
Figure 4.4.3-7. Osteogenic markers expression at different matrix stiffness.	124
Figure 4.4.3-8. Osteocalcin expression in disrupted contraction by construct attachment to the membrane.	125
Figure 4.4.3-9. Osteocalcin expression in disrupted contraction by addition of cell contractility inhibitor.	126
Figure 4.4.3-10. Glycosaminoglycans staining on MC3T3-E1 construct.	126
Figure 4.4.4-1. 3D image of cellular viability of a MC3T3-E1 construct.....	127

<i>Figure 4.4.4-2. Cellular viability at different matrix stiffness and media.</i>	128
<i>Figure 4.4.5-1. Final construct morphology depending on FBS concentration and PDGF addition.</i>	129
<i>Figure 4.4.5-2. Glycosaminoglycans staining on MC3T3-E1 constructs depending on the media supplements.</i>	130
<i>Figure 4.4.5-3. Expression of osteogenic markers in MC3T3E1 constructs cultured in 15 % FBS and PDGF.</i>	130
<i>Figure 4.4.5-4. Effect of pre-culture in 15 % FBS and PDGF on mineralization.</i>	131
<i>Figure 5.1.2-1. Distinct stages of chondrogenic differentiation.</i>	144
<i>Figure 5.1.2-2. Scheme of the extracellular matrix of mature chondrocytes.</i>	145
<i>Figure 5.4.1-1. General behavior of hNDF in RAD16-I self-assembling peptide hydrogel.</i>	154
<i>Figure 5.4.2-1. Glycosaminoglycans expression in hNDF and MEFs constructs.</i>	154
<i>Figure 5.4.3-1. Cell viability of hNDF within the self-assembling peptide hydrogel.</i>	155
<i>Figure 5.4.4-1. Calcium deposits around cell aggregates.</i>	156
<i>Figure 5.4.4-2. Bone markers expression during osteogenic differentiation of hNDF constructs.</i>	158
<i>Figure 5.4.5-1. Effect of FBS concentration, TGFβ3 and ascorbic acid on glycosaminoglycan secretion and calcification.</i>	159
<i>Figure 5.4.5-2. Effect of FBS concentration, TGFβ3, ITS and ascorbic acid on glycosaminoglycan secretion and calcification.</i>	159
<i>Figure 5.4.5-3. Aggrecan expression over time depending on chondrogenic supplements.</i>	160
<i>Figure 5.4.5-4. Compared aggrecan profile expression at 5 % and 2 % FBS in the complete chondrogenic medium.</i>	161
<i>Figure 5.4.5-5. Collagen type II expression at different serum concentration and chondrogenic supplements combinations.</i>	161
<i>Figure A2-1. Determination of the flow rate.</i>	175
<i>Figure A3-1. Representation of how micro-volume systems work.</i>	177
<i>Figure A4-1. Melting curves for qRT-PCR runs.</i>	182
<i>Figure A4-2. Graphical representation of qRT-PCR data.</i>	182
<i>Figure A4-3. Standard curve for 18s gene.</i>	183

LIST OF TABLES

<i>Table 1.1.3-1. Comparison of cell/tissue behavior under 2D and 3D culture conditions.</i>	8
<i>Table 2.3.2-1. Conditions of the functionalization of the PFM-containing samples.</i>	24
<i>Table 2.4.1-1. Experimental conditions for the bare PFM polymerization.</i>	28
<i>Table 2.4.1-2. High-resolution XPS scan data of the iCVD pPFM filma.</i>	30
<i>Table 2.4.1-3. Experimental conditions for the PFM-co-EGDA polymerization.</i>	31
<i>Table 2.4.2-1. XPS survey scan comparison of the peptide modified and the non-modified PFM.</i>	36
<i>Table 2.4.3-1. Experimental conditions of HEMA-co-EGDA-co-PFM polymerization.</i>	38
<i>Table 2.4.3-2. XPS survey scan before and after diamine reaction in PBS for the terpolymer.</i>	41
<i>Table 2.4.3-3. Spectroscopic ellipsometry analysis of the hydrogels with a PFM layer.</i>	43
<i>Table 2.4.3-4. XPS survey scan of PFM polymer and hydrogel/PFM samples.</i>	43
<i>Table 2.4.3-5. Angle-resolved XPS of hydrogels with PFM.</i>	44
<i>Table 2.4.4-1. Roughness data of the three different substrates.</i>	55
<i>Table 3.4.1-1. Comparison of ion concentrations in blood plasma, SBF and α-MEM.</i>	73
<i>Table 3.4.1-2. Solubilities of some of the biologically relevant calcium phosphates and carbonates.</i>	74
<i>Table 3.4.1-3. Equilibrium reactions in SBF.</i>	75
<i>Table 4.3.4-1. Formulation of three culture media: control, osteogenic and osteogenic with dexamethasone.</i>	105
<i>Table 4.3.9-1. List of the genes, abbreviations and catalog number.</i>	108
<i>Table 4.4.1-1. Self-assembling peptide concentrations and calculated G' values.</i>	110
<i>Table 5.3.6-1. List of primer sequences for chondrogenic and osteogenic genes and 18s, as reference.</i>	151
<i>Table A1-1. Standard aminoacid symbols and chemical structures.</i>	173
<i>Table A3-1. Some technical properties of low micro-volume systems.</i>	178
<i>Table A3-1. qRTPCR reaction setup for each test tube.</i>	180
<i>Table A4-1. qRTPCR cyler program.</i>	181

LIST OF ABBREVIATIONS

2D	Two-dimensional	HCM	Hepatocyte culture medium
3D	Three-dimensional	HEMA	2-Hydroxyethyl methacrylate
α -MEM	Alpha-minimum essential media	hNDF	Human normal dermal fibroblasts
α -TCP	Alpha-tricalcium phosphate	iCVD	Initiated chemical vapor deposition
β -GP	Beta-glycerophosphate	ITS	Insulin-transferrin-selenium supplement
β -TCP	Beta-tricalcium phosphate	MEF	Mouse embryonic fibroblast
ΔG	Variation of the Gibbs free energy	osteo	Osteogenic medium (with AA and β GP)
AA	Ascorbic acid	osteo+D	Osteogenic medium with dexamethasone (with AA, β GP and D)
AA2P	Ascorbic acid 2-phosphate	OC	Osteocalcin
ACP	Amorphous calcium phosphate	OCP	Octacalcium phosphate
AFM	Atomic force microscopy	OP	Osteopontin
ALP	Alkaline phosphatase	PBS	Phosphate buffered saline
BSP	Bone sialoprotein	PDGF	Platelet-derived growth factor-BB
C	Control medium	PFM	Pentafluorophenyl methacrylate
cHA	Commercial hydroxyapatite	PGs	Proteoglycans
COL1	Collagen type I, alpha 1	pPFM	Polymerized pentafluorophenyl methacrylate
COL2	Collagen type II, alpha 1	qRTPCR	Quantitative reverse transcriptase polymerase chain reaction
D	Dexamethasone	ROCK	Rho kinase
DAPI	4',6-Diamidino-2-phenylindole	SBF	Simulated body fluid
DCHP	Dihydrate calcium hydrogenphosphate	SEM	Scanning electron microscopy
DHA	Defective hydroxyapatite	sccm	Standard cubic centimeter per minute
ECM	Extracellular matrix	SCHA	Slightly carbonated apatite
EDS	Energy dispersive spectroscopy	SEM	Scanning electron microscopy
EGDA	Ethylene glycol diacrylate	sHA	Synthetic hydroxyapatite
FEG-SEM	Field emission gun – scanning electron microscopy	TBPO	tert-Butyl peroxide
FBS	Fetal bovine serum	TGF β 3	Transforming growth factor beta 3
FTIR	Fourier transform infrared spectroscopy	TRITC	Tetramethylrhodamine B isothiocyanate
GAGs	Glycosaminoglycans	XRD	X-ray diffraction
HA	Hydroxyapatite		
HCHA	Heavily carbonated apatite		

LIST OF PUBLICATIONS

RESEARCH PAPERS FROM THIS THESIS

O'Shaughnessy, W. S., **Marí-Buyé, N.**, Borrós, S., Gleason, K. K., *Initiated Chemical Vapor Deposition of a Surface-Modifiable Copolymer for Covalent Attachment and Patterning of Nucleophilic Ligands. Macromolecular Rapid Communications*, **28**, 1877-1882 (2007).

Marí-Buyé, N., O'Shaughnessy, W. S., Colominas, C., Semino, C. E., Gleason, K. K., Borrós, S., *Functionalized, swellable hydrogel layers as a platform for cell studies. Advanced Functional Materials*, **19**, 1276-86 (2009).

Marí-Buyé, N. & Semino, C. E., *Development of a three-dimensional bone-like construct in a soft self-assembling peptide matrix.* (Submitted)

Bussmann, B. M., Reiche, S., **Marí-Buyé, N.**, Meisel, J., Semino, C. E., *Chondrogenic potential of human dermal fibroblasts in a contractile soft self-assembling peptide hydrogel.* (In preparation)

OTHER RESEARCH PAPERS

Wu, J.*, **Marí-Buyé, N.***, Lopez, L., Fernández Muiños, M. T., Borrós, S., Favia, P., Semino, C. E., *Nanometric self-assembling peptide layers enhance CYP3A2 expression of primary rat hepatocyte sandwich cultures.* *Journal of Nanobiotechnology*, **8**, 29 (2010).

*equal contribution

BOOK CHAPTERS

Marí-Buyé, N., Fernández Muiños, M. T., Semino, C. E., *Three-dimensional cultures in soft self-assembling nanofibers.* In *Methods in Bioengineering: 3D Tissue Engineering* (2010). Series editors: Berthiaume, F. and Morgan, J. Artech House.

Marí-Buyé, N. & Semino, C. E., *Differentiation of mouse embryonic stem cells in self-assembling peptide scaffold.* In *Methods in Molecular Biology* **690**, 217-37 (2011). Series editor: Zur Nieden, N.I. The Humana Press Inc.

CHAPTER 1

INTRODUCTION TO CELL MICROENVIRONMENT AND BIOMIMETICS

1.1. BACKGROUND

1.1.1. BIOMIMETICS: LEARNING FROM NATURE

After millions of years of evolution, of selecting what works from what does not work, nature has optimized the design of its structures and the way to build them. Scientists have long envied nature's efficiency and elegance to develop the complex and sophisticated biological architectures, systems and functions. In the last decades, though, biologists, chemists, physicians and engineers, among others, have begun not only to learn more precisely about nature's strategies, but also to apply these new concepts to solve actual problems in many disciplines. This idea of "learning from nature" was designated as biomimetics, the synthesis of two words of Greek origin: *bios* (life) and *mimesis* (to imitate or mimic). Many other names are also used in the same sense, such as bionics, biomimicry or bio-inspiration.

One of the earliest and most famous examples of biomimetics is the invention of Velcro in 1941 by a Swiss engineer, who was inspired by the tiny hooks found on the surface of a burdock that easily attached to hair and fabrics (Figure 1.1.1-1). A more recent technological example is the bionic car created by DaimlerChrysler AG in 2005, which was modeled by mimicking the shape of a tropical fish (boxfish) in order to reduce fuel consumption and nitrogen oxide emissions¹.

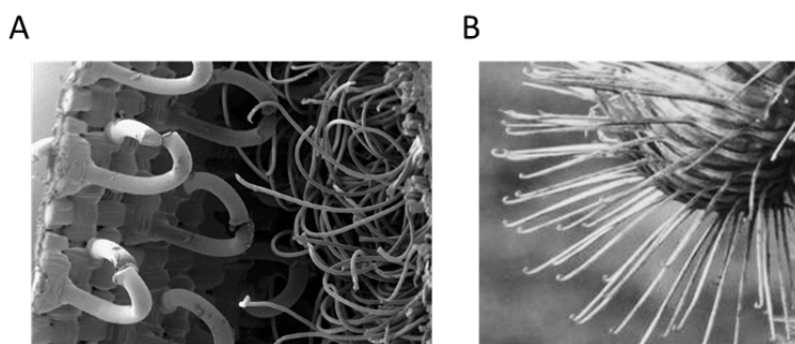


Figure 1.1.1-1. Comparison of Velcro structure with its natural analog, the burdock. (A) Velcro consists of thousands of small hooks that reversibly bind to tiny fuzzy loops². (B) This design imitates the hooks on burrs³, which are used as a natural mechanism for seed dispersion.

Nowadays, the concept of biomimetics also appears as an appealing and recurrent approach for bioengineers working in the field of tissue engineering and regenerative medicine. They use nature as a source of ideas to develop new biomaterials or strategies that could more precisely emulate the cellular environment as well as some aspects of the developmental processes *in vivo*. Nonetheless, these approaches firstly require a comprehensive insight into the natural environment of the cells.

1.1.2. AN OVERVIEW OF THE NATURAL CELL ENVIRONMENT

Any living tissue is made of individual cells, the fundamental units of life, which assemble interacting with one another, communicating, organizing themselves and, in short, working together to perform a particular function. Along with the neighboring cells, an intricate meshwork of large and small biological molecules that constitute the extracellular matrix (ECM) embeds the cells. Moreover, cells are also subjected to gradients of oxygen and nutrients, as well as to chemical stimuli of many other soluble factors and to external mechanical cues, such as flow or tension. All these factors, among others, are constantly influencing cell behavior *in vivo* and, conversely, cells are also able to modulate their local surroundings, which reflects the high complexity of the natural cell environment (Figure 1.1.2-1).

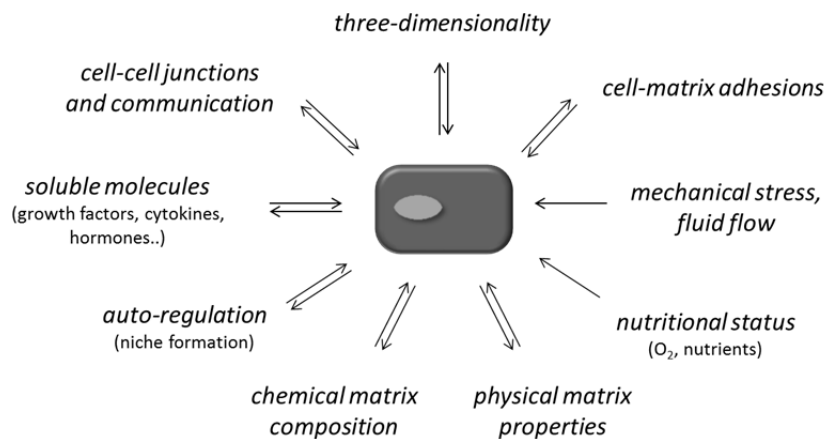


Figure 1.1.2-1. Microenvironmental factors affecting cell behavior. Many different biochemical and biophysical factors of the cell microenvironment modulate cell biology. Cells, in turn, modify their local environment, as well. Adapted from Yamada *et al.*⁴

The extracellular matrix: chemical composition and function

Broadly, the ECM is made up of fibrous proteins -mostly collagen, elastin, laminin and fibronectin- embedded in a jelly structure consisting of glycosaminoglycans (polysaccharide chains) -such as hyaluronic acid and heparan sulfate- and proteoglycans (complex macromolecules that contain a core protein with one or more covalently attached glycosaminoglycans) –such as aggrecan⁵. From the functional point of view, the glycosaminoglycan (GAG) and proteoglycan (PG) gel provides a hydrated space around cells that resists compression and regulates the transport of molecules between the blood stream and cells. At the same time, these polysaccharides are essential in the chemical signaling, since they sequester soluble biomolecules and can enhance or inhibit their signaling activity. Regarding fibrous proteins, collagen and elastin act as structural proteins and improve the mechanical properties of this gel-like matrix by conferring strength and elasticity, respectively. On the other hand, many other proteins, such as laminin and fibronectin, function as adhesive molecules, since they expose specific motifs that are recognized by the adhesion receptors (integrins) localized at the cell surface. A scheme of the mentioned ECM components is provided in Figure 1.1.2-2.

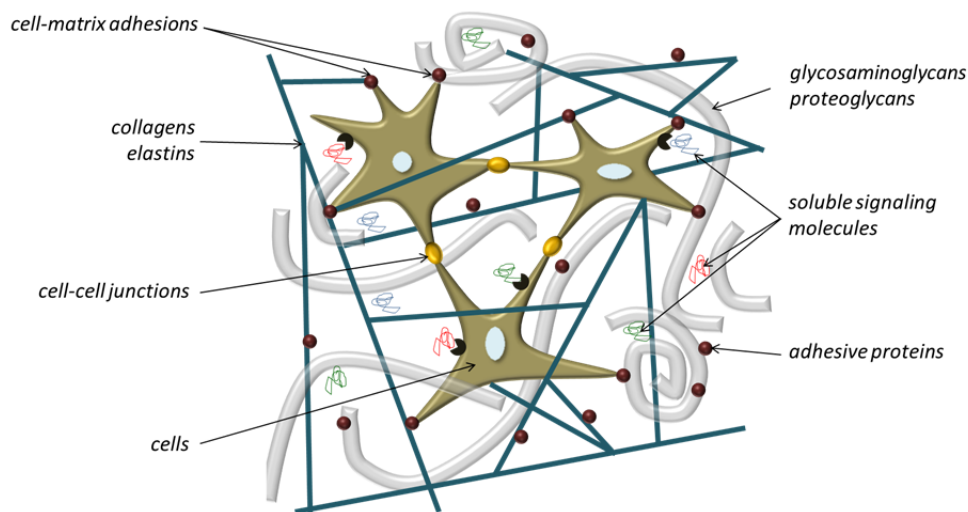


Figure 1.1.2-2. Scheme of the basic ECM components in the 3D environment of the cells. Tissue comprises a population of cells that interact with each other and also with the ECM components: adhesion and structural proteins and soluble biomolecules.

Actually, it is the own cell that locally secretes the whole variety of proteins and polysaccharides that, helped by the cells themselves, consecutively assemble into the organized ECM structure. Furthermore, cells also carry out the matrix degradation by secreting proteolytic enzymes, which enable cell migration and tissue remodeling. The extracellular matrix is, thus, a dynamic, highly hydrated and self-assembled three-dimensional network that not only works as a supporting framework for cells, but also plays a key role in cell regulation from migration and proliferation to differentiation or morphogenesis. It could be considered that the ECM composition is unique in each tissue or cellular niche, working as a specific tissue signature and maintaining the cellular identity and function in each environment. This regulation occurs not only due to the chemical cues -either from the ECM proteins or the tethered soluble molecules- but also due to the intrinsic biophysical properties of the matrix.

Biophysical properties of the ECM: cells sense the environment mechanics

Physical properties of many tissues are determined by the different combinations of the extracellular matrix components at the microscopic level and their hierarchical organization. For example, in tendons and ligaments, the tissue strength is clearly improved due to the parallel organization of collagen fibers⁶. In cartilage, instead, the high content in certain proteoglycans provides cushion and low friction to the tissue, as well as it favors the movement of nutrients in an environment with no vascularization⁷. On the other hand, the intimate association of collagen fibers with mineral nanocrystals and its hierarchical structure are responsible for the hardness and rigidity of bone tissue, with a crucial structural role, while still maintaining quiet an elastic behavior and a considerable intrinsic tensile strength⁸.

However, mechanical properties are not only relevant at the macroscopic tissue level, but they also have a fundamental role in regulating functions at the cellular level. Nowadays, it is well known that cells can push and pull within their environment through cell-matrix and cell-cell adhesions, so that

they feel the surrounding mechanical properties. Cells continuously exert forces on the matrix that are balanced, in turn, by the ECM depending on its intrinsic mechanical properties. Thus, cells sense the resistance opposed by the environment and respond by adjusting their adhesions, cytoskeleton, and overall state⁹. In fact, mechanical cues from the environment are proven to alter many physiological processes -migration, proliferation, differentiation and even disease development- that were generally thought to be only controlled by chemical stimuli¹⁰. Moreover, the ECM connects mechanically each cell of a tissue, creating a mechanical continuum, where forces and deformations are homogeneously transmitted across the tissue.

Cell-cell adhesions and communication

As mentioned above, cells bind directly not only to the ECM components, but also to other cells through specialized membrane proteins (cell-adhesion molecules), such as selectins, integrins or cadherins, forming transient and stable interactions⁵. The resulting cell coupling provides communication channels among cells that create a cytoplasmic continuity, allowing small signaling molecules to diffuse from one cell to another. As in cell-matrix adhesions, cell-cell adhesion molecules do not act only as binding proteins but also as signaling molecules that regulate survival and function in response to these contacts. Importantly, cell-cell interactions have a critical role in directing differentiation in embryonic development or in tissue morphogenesis, since they are involved in cell recognition and sorting, boundary formation, movement coordination, and induction and maintenance of cell and tissue polarity¹¹.

Obviously cell-cell communication does not only take place through direct cell binding, but also by recognition and binding of soluble signaling factors. These molecules can be secreted by the cell itself (autocrine signals) or by cells located in the close vicinity (paracrine signals) or far apart, in which case signaling molecules reach the target through the bloodstream (endocrine signals). By binding many of these soluble effectors, the ECM modulates their local concentrations and gradients, which implies high control on chemical signaling.

External factors: mechanical stress, oxygen and nutrients

Mechanical forces -beyond the closest cell microenvironment-, oxygen levels or nutrient concentrations are external factors that are not governed by the own cells, but they actively determine their behavior. *In vivo*, cells are subjected to a high variety of external physiological stresses; for instance, compression and hydrostatic pressure on chondrocytes in knee cartilage, shear stress over the endothelial cells of the arteries and veins due to blood flow, loading on bone cells and tension on tendon cells. These mechanical forces are transmitted to the cell microenvironment and condition cell behavior and, in turn, the development of the organism and its response to injury. As examples, gravitational force is known to control bone deposition, whereas isotonic tension makes muscles grow, or shear stress in arteries and veins prevents coagulation¹².

Regarding the nutritional status, in most of the tissues nutrients and oxygen are supplied to cells by means of an elaborate vascular system and subsequent diffusion -over diffusional transport distance. For instance, in the case of a highly vascularized tissue such as bone, vasculature is organized to ensure that every bone cell lies within 300 μm of a blood vessel¹³. Exceptionally, cartilage lacks direct vascular supply, thereby receiving the essential nutrients and oxygen from the neighboring synovial fluid as a result of diffusion¹⁴. As a consequence and opposed to bone cells, chondrocytes are characterized by low oxygen consumption and a slow metabolism, which hinders cartilage self-repair. Therefore, these cases exemplify the importance of oxygen levels for cell functions.

Bidirectional communication and auto-regulation of the cell microenvironment

As suggested in the previous overview of the cell microenvironment or niche, a higher order of organization exists beyond the cell. In the cell microenvironment, there is structural and functional continuity between cells cytoskeleton and matrix fibers¹⁵, which integrates cells into a larger system. Indeed, the whole system is regulated by a spatial and temporal coordination of many soluble effectors, as well as cell-cell and cell-matrix interactions. These interactions are, indeed, bidirectional: cells act on their surroundings and, in turn, they are influenced by the new environment. Thus, the behavior at the tissue level emerges from these multiple cellular interactions and interconnected regulatory feedback loops.

1.1.3. BIOMIMETICS IN TISSUE ENGINEERING: DECONSTRUCTING THE COMPLEX BIOLOGICAL ENVIRONMENT INTO SIMPLE SYSTEMS (MODELS)

Simplified models for tissue engineering

In 1993, Langer and Vacanti published a definition for tissue engineering that is still commonly applied and states that “tissue engineering is an interdisciplinary field that applies the principles of engineering and life sciences toward the development of biological substitutes that restore, maintain, or improve tissue function or a whole organ”¹⁶. In addition to the challenging therapeutic application of creating functional artificial tissues, engineered tissues also find application as platforms for pharmacological and physiological studies *in vitro*. In turn, these models provide valuable knowledge that helps to design better strategies for organs substitutes or grafts that could eventually be used in regenerative medicine.

In the late 1970s, first approaches to tissue engineering were based on the combination of cells with natural materials, in particular collagen, used as support for the growth of transplanted cells especially in the area of artificial skin¹⁷. Later, in the mid-80s, Langer and Vacanti started to use biocompatible synthetic polymers as cell scaffolds¹⁸, thereby opening new perspectives in tissue engineering and in the biomaterials field. During the next years, a lot of effort was focused on developing techniques to manufacture feasible three-dimensional polymeric scaffolds –such as

solvent casting and particulate leaching, melt molding or computer-guided solid free-form manufacturing¹⁹. Nonetheless, after many frustrated attempts in achieving an engineered tissue, it was evident that a lot of understanding on cell behavior was still required to advance in the field. Therefore, many researchers moved some steps backwards in order to design models that might help to comprehend and identify the factors that actually rule cell functions. Nowadays, this is still one important goal for many tissue engineers.

These *in vitro* models try to simplify the high complexity of the biological niche by mimicking key parameters that drive cellular response. For this purpose, it was important to deconstruct the cellular microenvironment into different elements (see again Figure 1.1.2-1) to analyze the effect of the distinct components, isolated or combined, in reductionist *in vitro* models.

2D versus 3D models

Although most cells perceive the environment in a three-dimensional (3D) manner *in vivo*, cells have been traditionally cultured on two-dimensional (2D) substrates. Indeed, 2D experiments provide a lot of valuable information on the relationship between cell functions and its surroundings. Nonetheless, these platforms present important limitations, because many essential cellular features and functions are actually altered or missed in 2D. Table 1.1.3-1 highlights some general discrepancies between 2D and 3D cultures, although exceptions exist (adapted from Geckil *et al.*²⁰).

Table 1.1.3-1. Comparison of cell/tissue behavior under 2D and 3D culture conditions^a.

feature / function	in 2D	in 3D
tissue-specific architecture	poor	rich
cell morphology ^b	flat, extended	round, contracted
interactions	limited	multiple
cell motility	fast, free	slow, restricted
cell adhesion	weak	strong
cell growth	directional	in all directions
cell proliferation	high	low
apoptosis	induced	tissue-like
intracellular stiffness	an order of magnitude higher in 3D	
cell polarization	partly	full
extracellular matrix remodeling	absent or poor	present
fluid perfusion	1D	3D
signaling and diffusion	asymmetric	nearly symmetric
metabolic rate	high	low
cell survival when exposed to cytotoxic agents	low	high

^a Adapted from Geckil *et al.*²⁰.

^b General cell shape, but depends on substrate stiffness both in 2D and 3D.

Many studies exemplify the dichotomy between 2D and 3D cultures. In general, adhesions to the matrix and cytoskeleton structures in 3D differ in structure, localization, and function compared to

2D²¹ (Figure 1.1.3-1 A). Moreover, cells in 3D models such as spheroids can re-establish multiple cellular interconnections in a 3D configuration that allow them to express a tissue-like phenotype²² (Figure 1.1.3-1 B). In contrast, cells in 2D are unnaturally polarized with a large area of their surface exposed to the culture medium and only in partial contact with the extracellular matrix (ECM) and adjacent cells (Figure 1.1.3-1 C). Anyhow, this 2D configuration could be a biomimetic model for epithelial cells that grow in sheets on flat basal lamina. Nonetheless, even these cells behave in a more realistic way when cultured in 3D gels of ECM, where they are capable to organize themselves into polarized structures such as hollow cysts and tubules²³ (Figure 1.1.3-1 D). This case illustrates the potential of 3D systems to allow morphogenesis and possible tissue formation. Another practical example is found in drug testing *in vitro*. 3D models seemed to more closely predict cell response to the therapeutic agent, as they recreate environmental cues that simple 2D cultures cannot. In the particular case of tumor models, angiogenic capacity of tumoral cells *in vivo* can be mimicked in 3D hydrogels where cells showed enhanced malignant potential and less sensitivity to chemotherapy²⁴.

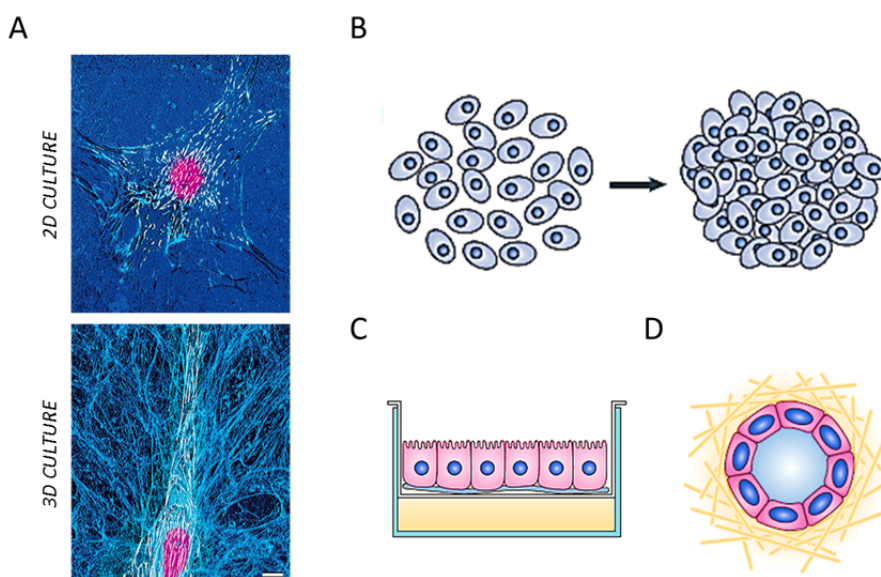


Figure 1.1.3-1. 2D versus 3D cultures. (A) Distinct overall morphology of human fibroblasts in a 2D microenvironment –on planar fibronectin- versus a 3D microenvironment –within a mesenchymal cell-derived 3D matrix. White scale bar = 10 μm . From Yamada *et al.*⁴ (B) 3D culture in spheroids. (C) Epithelial cells grown at the air–medium interface on porous membranes form polarized monolayers cultured on 2D membranes. (D) Epithelial cells grown in 3D collagen gel yield spherical monolayered cysts, which are fully polarized. (B, C, D) adapted from Pampaloni *et al.*²²

Indeed, the third dimension is required in order to capture the physiological cell responses and bridge the gap between simplistic 2D cultures and extremely complex animal models^{4,25}. Therefore, researchers are shifting their attention in developing reliable and controllable 3D culture systems. Nonetheless, 3D cultures are simplifications that cannot completely recreate the cellular microenvironment, but still too complex to fully understand and control every variable. Therefore, traditional 2D cultures are still very useful to elucidate cell behavior indeed.

1.2. MOTIVATION AND GENERAL AIMS

The present work explores different platforms or models both in two- and three-dimensions intended for tissue engineering applications. Each of them tries to recapitulate one or more parameters of the cell microenvironment, in order to obtain more or less complex biomimetic approaches for general cell studies or bone and cartilage tissue engineering. Hence, this work is motivated by the concept of “learning from nature”. Literally, by studying the natural environment of the cells or even strategies in tissue development, it should be possible to produce new enhanced materials or more successful cellular models or engineered tissues.

In particular, the aims of the present thesis can be summarized in the following points:

- (1) To design and develop a two-dimensional platform for basic cell studies combining controlled chemical and mechanical properties in order to mimic signaling from the extracellular matrix (Chapter 2).
- (2) To compare the biomimetic interaction of both synthetic and commercial hydroxyapatite surfaces with physiological media and evaluate their *in vitro* performance in terms of bioactivity and eventual formation of biomimetic apatite (Chapter 3).
- (3) To develop a three-dimensional biomimetic model for bone tissue engineering that mimics cellular interactions in a real 3D environment, as well as recreates early stages of bone formation (Chapter 4).
- (4) To obtain a three-dimensional biomimetic model for artificial cartilage from human dermal fibroblasts (Chapter 5).

1.3. CONTENT OF THIS DISSERTATION

The two first chapters of this thesis are primarily focused on materials development on surfaces (2D), whereas the last two chapters are 3D models aimed for tissue engineering applications. Overall, each chapter may be considered as an independent research focused in the exploration of a particular topic.

Chapter 2 presents the development of a 2D model envisioned to mimic both chemical and physical signaling from the extracellular matrix. For this purpose, thin polymeric layers combining tunable chemical and mechanical properties were designed. The films were produced and characterized in Prof. Karen K. Gleason’s Group at the Massachusetts Institute of Technology (MIT), who is the inventor of a technology called initiated chemical vapor deposition (iCVD). The conceptual design, the experimental process for film deposition and characterization are detailed in this chapter, along

with preliminary studies with cells, which were partly conducted at the Center for Biological Engineering at MIT.

In the particular field of bone tissue engineering, apatitic surfaces on biomaterials have an important role in bone integration. Chapter 3 evaluates the possibility to form a biomimetic apatite layer –with composition similar to that found in bone- on an in-house synthesized hydroxyapatite surface, compared to a commercial one. The interaction of these ceramics with physiological media was studied, both theoretically and experimentally, as well as the mechanism by which a bone-like apatite might be achieved. This chapter adds insight into other works of the group that suggested the benefits of this synthetic ceramic for bone formation.

Nonetheless, a three-dimensional environment is certainly required for final tissue engineering applications. Therefore, Chapter 4 describes a three-dimensional biomimetic model for bone tissue engineering, where cellular connections in a real 3D conformation are mimicked, as well as certain stages of bone development. For this purpose, the suitability to use a soft self-assembling peptide hydrogel as scaffold was evaluated. The effect of different matrix stiffness on cellular morphology and cell-cell interconnection was studied, as well as the osteogenic differentiation of mouse osteoprogenitor cells. Part of this work was performed at the Translational Center for Regenerative Medicine (TRM) of the University of Leipzig (Germany).

Finally, Chapter 5 explores the potential of human dermal fibroblasts to produce a cartilage-like construct, based on the model described in Chapter 4. As for bone engineering, the initial culture conditions provided a real 3D environment to the cells and allowed the recreation of chondrogenic development stages. Troubleshooting and culture conditions in this system are discussed. Part of the experimental procedures in this chapter was conducted by Bianca Bussmann and Sven Reiche at the Translational Center for Regenerative Medicine of the University of Leipzig.

1.4. REFERENCES

1. Phenix, M. *CNN Tech - Mercedes' fish-inspired car*. March 2007 - last update (http://articles.cnn.com/2007-03-08/tech/cars.fish.popsi_1_fish-inspired-concept-car-small-cars?_s=PM:TECH).
2. Mesghali, E. *Biomimetic architecture - Velcro fastening*. September 2009 - last update (<http://biomimetic-architecture.com/2009/09/06/stick-like-a-burr/>).
3. Cane, J. *Botanical Velcro aids seed dispersal*. 2010 - last update (<http://www.bridgerlandaudubon.org/wildaboututah/101007botanicalvelcro.htm>).
4. Yamada, K. M. & Cukierman, E. *Modeling tissue morphogenesis and cancer in 3D*. *Cell* **130**, 601-610 (2007).
5. Alberts, B., Alexander, J., Lewis, J., Raff, M., Roberts, K. & Walter, P. in *Molecular Biology of the Cell* (Garland Science, New York and London, 2004).
6. Kjaer, M. *Role of extracellular matrix in adaptation of tendon and skeletal muscle to mechanical loading*. *Physiol. Rev.* **84**, 649-698 (2004).
7. Hall, B. K. & Newman, S. A. in *Cartilage: molecular aspects* (CRC Press, Boca Raton, United States, 1991).
8. Bilezikian, J., Raisz, L. & Martin, T. in *Principles of bone biology* (Elsevier, Amsterdam, 2008).
9. Discher, D. E., Janmey, P. & Wang, Y. L. *Tissue cells feel and respond to the stiffness of their substrate*. *Science* **310**, 1139-1143 (2005).
10. Janmey, P. A. & Miller, R. T. *Mechanisms of mechanical signaling in development and disease*. *J. Cell. Sci.* **124**, 9-18 (2011).
11. Halbleib, J. M. & Nelson, W. J. *Cadherins in development: cell adhesion, sorting, and tissue morphogenesis*. *Genes Dev.* **20**, 3199-3214 (2006).
12. Chen, C. S., Tan, J. & Tien, J. *Mechanotransduction at cell-matrix and cell-cell contacts*. *Annu. Rev. Biomed. Eng.* **6**, 275-302 (2004).
13. Buckwalter, J. A., Glimcher, M. J., Cooper, R. R. & Recker, R. *Bone biology. I: Structure, blood supply, cells, matrix, and mineralization*. *Instr. Course Lect.* **45**, 371-386 (1996).
14. Buckwalter, J. A. & Mankin, H. J. *Articular cartilage: tissue design and chondrocyte-matrix interactions*. *Instr. Course Lect.* **47**, 477-486 (1998).
15. Ingber, D. E. *Cellular mechanotransduction: putting all the pieces together again*. *FASEB J.* **20**, 811-827 (2006).
16. Langer, R. & Vacanti, J. P. *Tissue engineering*. *Science* **260**, 920-926 (1993).
17. Yannas, I. V. & Burke, J. F. *Design of an artificial skin. I. Basic design principles*. *J. Biomed. Mater. Res.* **14**, 65-81 (1980).
18. Vacanti, J. P., Morse, M. A., Saltzman, W. M., Domb, A. J., Perez-Atayde, A. & Langer, R. *Selective cell transplantation using bioabsorbable artificial polymers as matrices*. *J. Pediatr. Surg.* **23**, 3-9 (1988).

19. Murphy, M. B. & Mikos, A. G. in *Principles of tissue engineering* (eds Lanza, R., Langer, R. & Vacanti, J. P.) (Elsevier Inc., Burlington MA, USA, 2007).
20. Geckil, H., Xu, F., Zhang, X., Moon, S. & Demirci, U. *Engineering hydrogels as extracellular matrix mimics*. *Nanomedicine (Lond)* **5**, 469-484 (2010).
21. Cukierman, E., Pankov, R., Stevens, D. R. & Yamada, K. M. *Taking cell-matrix adhesions to the third dimension*. *Science* **294**, 1708-1712 (2001).
22. Pampaloni, F., Reynaud, E. G. & Stelzer, E. H. *The third dimension bridges the gap between cell culture and live tissue*. *Nat. Rev. Mol. Cell Biol.* **8**, 839-845 (2007).
23. Zegers, M. M., O'Brien, L. E., Yu, W., Datta, A. & Mostov, K. E. *Epithelial polarity and tubulogenesis in vitro*. *Trends Cell Biol.* **13**, 169-176 (2003).
24. Fischbach, C., Chen, R., Matsumoto, T., Schmelzle, T., Brugge, J. S., Polverini, P. J. & Mooney, D. J. *Engineering tumors with 3D scaffolds*. *Nat. Methods* **4**, 855-860 (2007).
25. Griffith, L. G. & Swartz, M. A. *Capturing complex 3D tissue physiology in vitro*. *Nature Reviews Molecular Cell Biology* **7**, 211-224 (2006).

CHAPTER 2

BIOMIMETIC POLYMERIC THIN FILMS COMBINING BIOCHEMICAL AND BIOPHYSICAL PROPERTIES

2.1. BACKGROUND

2.1.1. OVERVIEW

Although cells generally perceive the environment in a three-dimensional (3D) manner *in vivo*, they have been traditionally cultured on two-dimensional (2D) substrates. Indeed, 2D experiments provide a lot of valuable information on the relationship between cell functions and its surroundings. For many decades, soluble biomolecules, such as growth factors, cytokines or hormones, have been typically used to trigger specific cellular responses *in vitro* and their effects have been extensively characterized. Along with soluble molecules, proteins of the extracellular matrix (ECM) also play a critical role in cellular behavior. Therefore, many strategies have been developed to elucidate the instructive cues from the ECM by immobilization of proteins, short peptides or saccharides on 2D substrates. The incorporation of these approaches to tissue engineering produced a new generation of biomimetic scaffolds, which could better recreate certain aspects of the cell microenvironment. However, nowadays it is well established that the physical properties of the surroundings can be as influential as chemical factors. Hence, there is growing interest among scientist in exploring more sophisticated platforms that might be able to combine both chemical and physical signaling and, thus, produce more biomimetic surfaces.

2.1.2. HOW CELLS SENSE THE ENVIRONMENT

Cells are continuously sensing and responding to signals from the extracellular matrix (ECM). Integrins are the primary cell surface receptors that are responsible for cell–matrix adhesion and they bind to a large number of extracellular matrix proteins (collagens, fibronectins, fibrinogen, laminins, bone matrix proteins, etc.)¹. Integrin binding to ECM ligands lead to the clustering of other specialized proteins and remodeling of the cellular cytoskeleton, forming the so-called focal adhesion complexes (Figure 2.1.2-1). These changes caused by specific cell-ECM interactions are immediately transduced into biochemical signals. Cells are sensitive to the type of ligand and concentration, which induce distinct cellular signals and, in turn, control many cellular processes aside adhesion, for instance, migration, proliferation, survival and apoptosis, gene expression and differentiation²⁻⁴.

Nonetheless, cells do not only adhere to the surrounding environment, but also mechanically interact with it in a process known as mechanotransduction that also occurs at cell-cell contacts⁵. As observed in Figure 2.1.2-1, actin filaments are coupled to the ECM fibers via focal adhesion complexes, creating a cytoskeleton-ECM continuity that provides the basis of the bidirectional communication between cell and matrix. Cells are known to exert traction to the microenvironment by pulling and pushing on the ECM. Conversely, the ECM balances this stress and feeds back to alter cell shape and function

depending on its ability to resist cellular traction⁶. As chemical signaling, mechanical interaction is known to provide instructive signals that dictate cell behavior⁷.

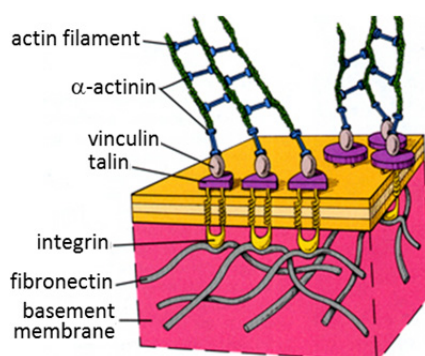


Figure 2.1.2-1. Basic components of the focal adhesion complexes. The extracellular domain of integrins binds matrix proteins, while the cytosolic domain interacts with the intracellular proteins and, thus, with the cytoskeleton. From the Indiana University - Purdue University Indianapolis⁸.

2.1.3. MODELS MIMICKING CHEMICAL SIGNALING

Many different strategies have been developed in order to mimic the chemical signaling from the extracellular matrix (ECM). Originally, inert materials were simply coated with ECM proteins, such as collagen, fibronectin or laminin, in order to improve cell adhesion. Since only a specific part of the proteins acts as binding ligand, the immobilization of these peptide fragments on surfaces has been widely used to imitate the cellular environment and, thus, study cellular behavior. The classical example is the integrin-binding RGD (arginine-glycine-aspartic acid) motif from fibronectin and laminin that clearly promotes cell adhesion and migration⁹. Many other biologically active motifs have been found to induce other functions, such as FHRRIKA –a heparin-binding domain that enhanced osteoblast mineralization when combined with RGD¹⁰- or IKVAV –a laminin domain that improves neurite extension¹¹. More recently, high-throughput screening and combinatorial techniques help to investigate the best combinations of both soluble and tethered chemical signals to develop artificial microenvironments¹².

Cells respond not only to the adhesion sequences itself, but also to their density and spatial presentation. For instance, adhesion and migration speed of murine fibroblasts were found to be dependent on both size and average density of integrin-binding clusters at the nanoscale level¹³. Moreover, the presentation of distinct integrin-binding ligands synergize to enhance adhesion, intracellular signaling and proliferation, as observed in the combination of two fragments from collagen type I and fibronectin that target different integrins¹⁴.

2.1.4. IMPACT OF MATRIX PHYSICAL PROPERTIES ON CELL FUNCTION

In addition to chemical composition, physical properties of the scaffold (roughness, topography, stiffness, etc.) clearly influence cell function. For instance, osteoblasts rather adhere and proliferate

on rougher substrates, whereas fibroblasts show the opposite behavior¹⁵. Moreover, topography at the micro- and nanoscale can guide migration¹⁶ or modulate osteogenic differentiation as function of pattern symmetry and disorder¹⁷. Recently, matrix stiffness has also been defined as a potent regulator of cell phenotype. In fact, the capability of the extracellular matrix to balance cell traction is directly link to the stiffness of the matrix. In general, a relatively stiff substrate resists cellular forces more than a soft one, causing the cell to spread better on the surface and grow¹⁸. In contrast, soft matrices promote cell retraction, turn off growth and could switch on differentiation⁶.

Indeed, several studies in the last decade reported distinct cell behaviors on stiff and soft substrates. Fibroblasts and epithelial cells, for example, were observed to spread better on stiff substrates than on softer ones, where they adopt a more spherical shape¹⁹. On the contrary, neurons seemed to survive better on soft surfaces, where they rather develop extensive and branched neurites compared to rigid substrates²⁰. Also capillary morphogenesis depends on substrate flexibility, as endothelial cells tend to form long capillary-like tubular structures in compliant collagen or synthetic self-assembling peptide gels, whereas in stiffer matrices they tend to spread and present less branching²¹. In contrast, other cell types, such as neutrophiles, seemed not to respond to substrate compliance²². Other studies show that it is even possible to distinguish between cell phenotypes depending on the stiffness of the surface, as illustrated by soft agar that is used to grow and identify cancer cells²³. Well-known work by Engler *et al.* proved that matrix stiffness is able to drive mesenchymal stem cell differentiation in a more selective way than soluble induction factors: soft gels that mimic brain induce neurogenic markers, stiffer ones that mimic muscle lead to myocytes and more rigid matrices that imitate bone promote the expression of osteogenic genes²⁴. The impact of stiffness is such that unusual high stiffness is actually associated to disease or scars. For instance, scar-like stiffness has been found to favor abnormal characteristics on glial cells²⁵ and cardiomyocytes²⁶. Even tumors are characterized by matrix stiffening, which is known to promote breast cancer progression²⁷.

2.1.5. MODELS COMBINING CHEMICAL AND MECHANICAL SIGNALING

Several systems have been developed in order to study the specific effects of matrix stiffness on cell functions. Typically, the elasticity of the extracellular matrix has been imitated by using 2D hydrogel substrates made of synthetic polymers. In particular, polyacrylamide (PA) gels have the most widespread usage. In this system, the stiffness can be easily tuned using different concentrations of crosslinking agent. Unlike natural matrices, these polymers are chemically stable, biologically inert and anti-adherent to serum proteins²⁸, which opens the possibility to separate chemical from mechanical signals. Nevertheless, the inertness of these materials might turn into an inconvenience, as it is harder to covalently attach molecules to act as ligands for cells. So far, these polymers are typically covered with a layer of extracellular matrix protein in order to promote cell adhesion. Collagen type I is the most commonly used^{19,24}, but many other ECM proteins have also been reported: fibronectin²⁹, collagen type V³⁰, laminin³¹, etc. Similar alternatives to PA gels are

polydimethylsiloxane (PDMS) or poly(ethylene glycol) (PEG) gels, the latter ones allowing the covalent immobilization of biomolecules within the gel³². Indeed, the possibility to covalently attach the bioactive molecules would raise the potential of the platform, since the range of possible ligands would extend to peptides and other small molecules, that otherwise could not be immobilized. In addition, ligand attachment only to the surface would concentrate the molecules and increase the efficiency of the system.

Different surface modifications have been applied to hydrogels in order to covalently immobilize biomolecules. Burnham *et al.*, for instance, conjugated polyacrylamide hydrogels with streptavidin by providing reactive sulfhydryl groups on the surface and subsequent reaction with a SH-reactive biotinylated linker³³. Others presented more complex strategies involving nanolithography to arrange gold nanoparticles on PEG surface that can be used to anchor thiol-terminated biomolecules³⁴. In general, surface modification of hydrogels requires several steps or relatively complex chemistry.

2.1.6. SINGLE-STEP FUNCTIONALIZATION: PENTAFLUOROPHENYL METHACRYLATE

In the group, pentafluorophenyl methacrylate (PFM) has been widely investigated as an active precursor for biomolecules binding³⁵⁻³⁸. PFM is an active ester that easily reacts with amines, which are highly abundant in biological ligands (i.e. small peptides and proteins). The free amine attacks the acyl group to render the corresponding amide and the leaving group pentafluorophenol (Figure 2.1.6-1). The reactivity of PFM towards amines was pointed out in bulk PFM polymers³⁹, but it has been extensively characterized on plasma-polymerized PFM surfaces. Primary amines have been determined to be more reactive towards the ester group than secondary and tertiary amines³⁷. More importantly, water also reacts with PFM leading to the cleavage of the pentafluorophenyl group and formation of the acid, a reaction that is accelerated in phosphate buffer saline (PBS)^{36,37}. Nevertheless, the amine substitution of the ester is always faster than hydrolysis in water, regardless of the solvent (deionized water or PBS), and it occurs at higher rate when amine is dissolved in PBS^{36,37}.

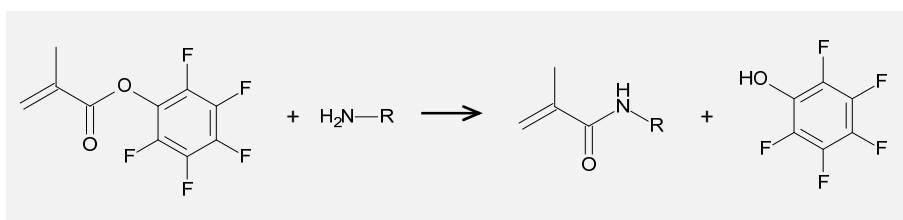


Figure 2.1.6-1. Pentafluorophenyl methacrylate structure and reactivity. The amine (nucleophile) attacks the active ester in a nucleophilic acyl substitution to form the corresponding amide.

Hence, PFM monomer provides an easy and fast way to attach amine-containing biomolecules under mild conditions to produce biologically tailored materials. Moreover, the coupling of PFM with a hydrogel might provide an equivalent platform to polyacrylamide gels with increased versatility. However, this combination might be difficult to achieve in solution due to the distinct solubility of

PFM –highly hydrophobic- and the monomers constituting the hydrogel that must be hydrophilic. Therefore, surface modification techniques, such as chemical vapor deposition, are envisioned as an alternative approach to develop polymeric layers.

2.1.7. INITIATED CHEMICAL VAPOR DEPOSITION (iCVD)

Initiated chemical vapor deposition (iCVD) is a one-step synthesis technique that produces polymer thin films on two- or three-dimensional objects from precursors in the vapor phase. iCVD is a subset of hot-filament CVD (HFCVD), which specifically uses a free radical initiator in order to decrease the filament temperature and enhance the deposition rate of the polymerization. Hence, iCVD presents the advantages of any vapor deposition, such as the avoidance of solvents and the formation of uniform coatings on substrates with complex geometries, but at the same time low filament temperatures promote selective chemistry by avoiding undesired chemical reactions such as the loss of monomer pendant groups. From this point of view, this technique is also a good alternative to plasma polymerization, where secondary reactions and damage of delicate organic moieties are usually a matter of concern.

As previously mentioned, iCVD involves the thermal decomposition of an initiator and subsequent free radical polymerization of the monomer to form a film on a cooled substrate. Basically, the initiator and the monomer species are vaporized and introduced in a vacuum chamber equipped with an array of heated filament wires, suspended above a backside-cooled substrate. A scheme and a picture of a reactor identical to the one used in this work is shown in Figure 2.1.7-1 A and B.

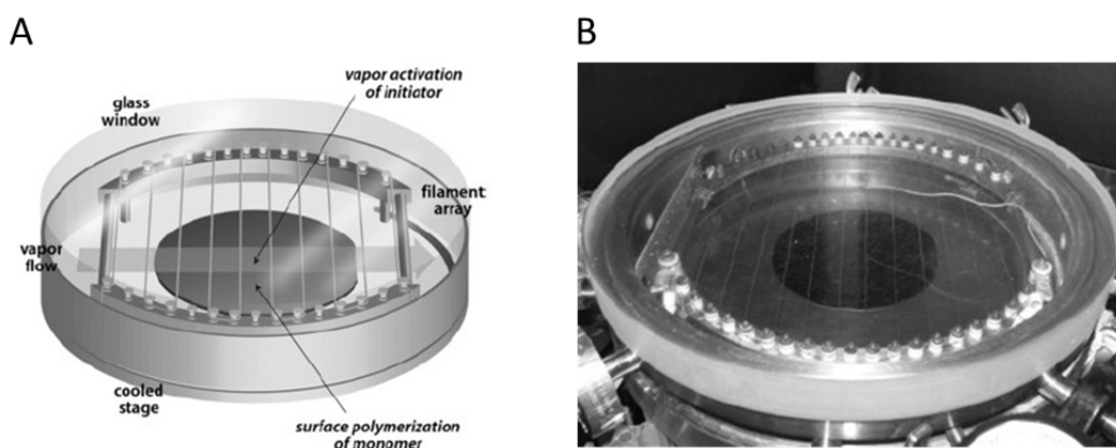


Figure 2.1.7-1. iCVD reactor setup. (A) Scheme and (B) picture of the reactor used to coat flat surfaces. The monomer and initiator vapors flow across an array of heated filaments above the substrate that is in contact with a cooled stage. The glass lid facilitates real-time monitoring. Illustration from Lau *et al.*⁴⁰.

The reaction mechanism proposed for iCVD polymerization can be broken down into a sequence of three reaction steps (Figure 2.1.7-2 A):

- (1) *Initiator decomposition*: firstly the initiator (I) is thermally decomposed in the vapor phase to form primary radicals.

- (2) *Primary radical and monomer adsorption*: the initiator radicals and the monomers (M) diffuse and adsorb from the vapor phase onto a surface.
- (3) *Surface polymerization*: finally the polymer (P) is formed by following the events in a usual free-radical polymerization: initiation, propagation and termination.

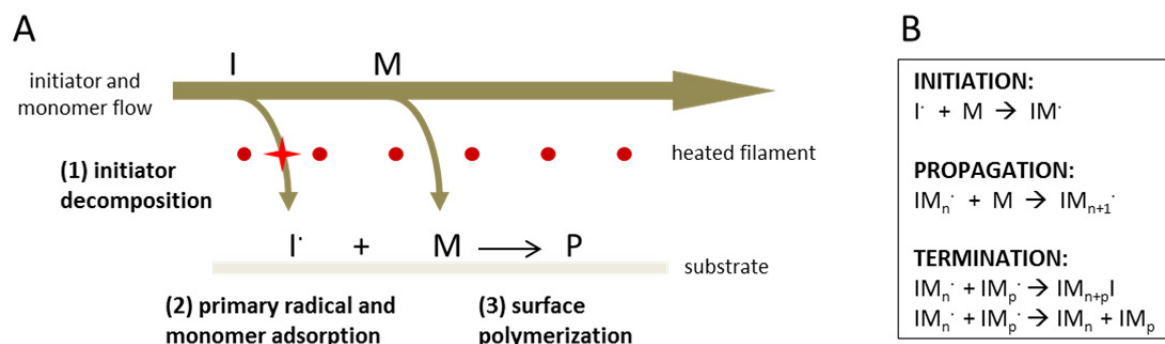


Figure 2.1.7-2. Reaction mechanism of a polymerization by iCVD. **(A)** Scheme of the three reaction steps: initiator (I) decomposition over the heated filament, adsorption of the radicals and the monomer (M) on the surface and free-radical polymerization to form the polymer (P). **(B)** Free-radical polymerization steps: initiation, propagation and termination.

As summarized by the reactions in Figure 2.1.7-2 B, the proper polymerization is started by the initiator radicals, which attack the vinyl bonds of the monomers. Next, the monomer molecules are successively added to the growing chain until annihilation of the radicals is produced by coupling or disproportionation. Consequently, a continuous stoichiometric polymer coating that resembles addition polymer from solution is obtained.

The stoichiometry of the final copolymer depends on the amount of each monomer adsorbed on the surface that, in turn, is determined by two factors: the partial pressure of the monomers in the reactor chamber (P_M) and their saturation pressure (P_{sat}) at the temperature of the polymerization, which is the temperature of the substrate. It was previously reported that the ratio P_M/P_{sat} can be qualitatively used as a measure of the amount of monomer adsorbed on the surface and it is recommended to keep it around 0.4 - 0.7⁴⁰. Lower values imply a poorer deposition rate; whereas if $P_M = P_{sat}$, the monomer condensates on the substrate, instead of polymerizing. Furthermore, the molecular weight of the final polymer can be also controlled by adjusting both the initiator to monomer ratio and the temperature of the filament⁴¹. Commonly, *tert*-butyl peroxide (TBPO) is used as initiator, since it easily dissociates at low temperatures (< 200 °C).

The iCVD technique was firstly developed and described by Karen K. Gleason's group at Massachusetts Institute of Technology in 2001. Her group studied its mechanism in detail^{40,42-44} and proved the synthesis of many different polymers from vinyl containing monomers, such as poly(2-hydroxyl methacrylate) and its copolymers⁴⁵, poly(methyl methacrylate)⁴⁶, poly(glycidyl methacrylate)⁴¹, poly(tetrafluoroethylene)⁴⁷ and fluorocarbon-organosilicon copolymer⁴⁸.

2.2. HYPOTHESIS AND SPECIFIC AIMS

The motivation of this chapter is to develop a polymeric thin hydrogel with tunable physical properties and functionalization capacity with bioactive motifs. The goal is, thus, to combine the pentafluorophenyl methacrylate (PFM) monomer with a hydrogel based on 2-hydroxyl methacrylate (HEMA). The production of these hydrogels with tailored swelling capacities by iCVD technique has been already described⁴⁵. Instead, PFM polymerization was never attempted by this technique. Hence, the first hypothesis of this work is that iCVD could be a suitable technique for the one-step synthesis of PFM-containing hydrogels. Secondly, these complex films, combining a hydrogel substrate and bioactive molecules, might be used as platform to study cell behavior under different chemical and physical signaling.

Therefore, the specific aims of this chapter are the following:

- (1) To synthesize and characterize PFM-based polymeric films by iCVD technique and corroborate the reactivity of these surfaces against aminated molecules.
- (2) To design, develop and characterize an innovative nanostructured surface polymer by iCVD, combining a hydrogel with tunable crosslinking densities –made out of HEMA and a crosslinker- with a monomer for aminated-molecules attachment (PFM).
- (3) To design peptide motifs with biological activity, ensure their attachment to the new surfaces and test the instructive capacity of the functionalized surfaces on cells.

2.3. MATERIALS AND METHODS

2.3.1. ICVD POLYMERIZATION

Polymer films were deposited on 100-mm-diameter silicon (Si) substrates in a custom-built vacuum reactor. The cylindrical reactor (height of 3.3 cm and radius of 12 cm) was covered with a quartz top that allowed laser interferometry (633 nm He-Ne laser source, JDS Uniphase) for real-time monitoring of the thickness. The reactor was equipped with a Nichrome filament (80% Ni / 20% Cr, AWG26, Omega Engineering) that was resistively heated at 280 °C. Filament temperature was measured by a thermocouple (Type K, AWG 36, Omega Engineering) directly attached to one of the wires. The silicon substrates were placed on a backside-cooled stage at 32 °C. Pressure in the vacuum chamber was varied depending on the experiment (200 - 250 mTorr) using a butterfly valve.

The monomers 2-hydroxyethyl methacrylate (HEMA, Aldrich) and pentafluorophenyl methacrylate (PFM, Polysciences) and the crosslinker ethylene glycol diacrylate (EGDA, Polysciences) were heated

and delivered into the reactor by using regulated needle valves (see chemical structure of the monomers in Figure 2.3.1-1). Meanwhile, the initiator *tert*-buthyl peroxide (TBPO, Aldrich) was vaporized at room temperature and metered into the chamber through a mass-flow controller, as well as nitrogen gas. The flow rates are expressed in sccm (standard centimeter cubic per minute) and calculated as indicated in Appendix 2. HEMA was always maintained at 65 °C, whereas the EGDA temperature was varied from 50 to 60 °C, according to the degree of crosslinking desired. PFM was heated up from 50 to 70 °C, depending on the flow needed. All vapors were mixed together before entering the reactor through a side port.

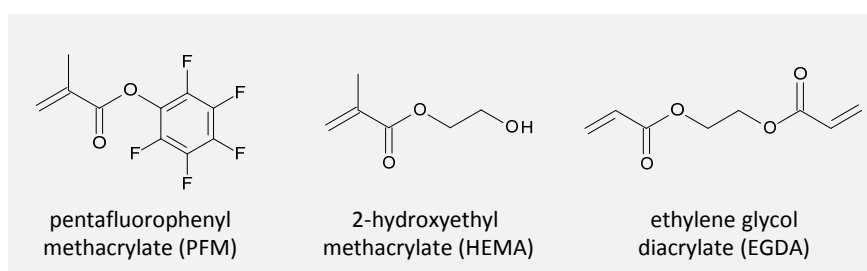


Figure 2.3.1-1. Chemical structure of the monomers. HEMA forms the hydrogel, PFM is the reactive molecule and EGDA acts as crosslinker.

2.3.2. SAMPLE REACTIVITY

PFM-containing samples were functionalized with various amine-containing molecules: 1,6-diaminohexane (Aldrich), fluorescein-5-thiosemicarbazide (FTSC, Molecular Probes) and peptides with the following sequences: RYVVLPR, GRGDSPY-FITC and GRADSPY-FITC (Biopolymer Facility at MIT), the last two carrying a fluorescein label (FITC) at the C-terminal. Three solvents were used: phosphate buffered saline (PBS, Aldrich), *N,N*-dimethylformamide (DMF, Aldrich) and ethanol (Aldrich). The samples were immersed in the corresponding solution, left on a shaker for 12 h (unless otherwise stated), rinsed twice in ethanol and water, and finally dried. The conditions of the different reactions are summarized in Table 2.3.2-1.

Table 2.3.2-1. Conditions of the functionalization of the PFM-containing samples.

reagents	media	concentration	temperature
1,6-diaminohexane	PBS and DMF / ethanol (10:90)	10 mM and 100 mM	room T and 60 °C
peptides	PBS	1 mM	37 °C
FTSC	ethanol	0.5 mM	60 °C

2.3.3. SURFACE CHARACTERIZATION

X-ray photoelectric spectrometry (XPS)

XPS was carried out on a Kratos Axis Ultra spectrometer using a monochromatized Al K α source. Spectra were usually recorded using a 70° take-off angle (θ) relative to the sample surface. For angle-resolved XPS, results were obtained at take-off angles of 20° and 90°, which is achieved by tilting the samples, as exemplified in Figure 2.3.3-1. The variation of the take-off angle allows studying the elemental composition depending on the depth. At 90° the X-ray is perpendicular to the surface and, thus, penetrates deeper into the film than at 20°. Therefore, lower angles provide additional near surface sensitivity. Deconvolution of the signals was performed in CASA XPS software, with relative sensitivity factors (RSF) of 0.278 for C, 0.780 for O, 1.000 for F and 0.477 for N.

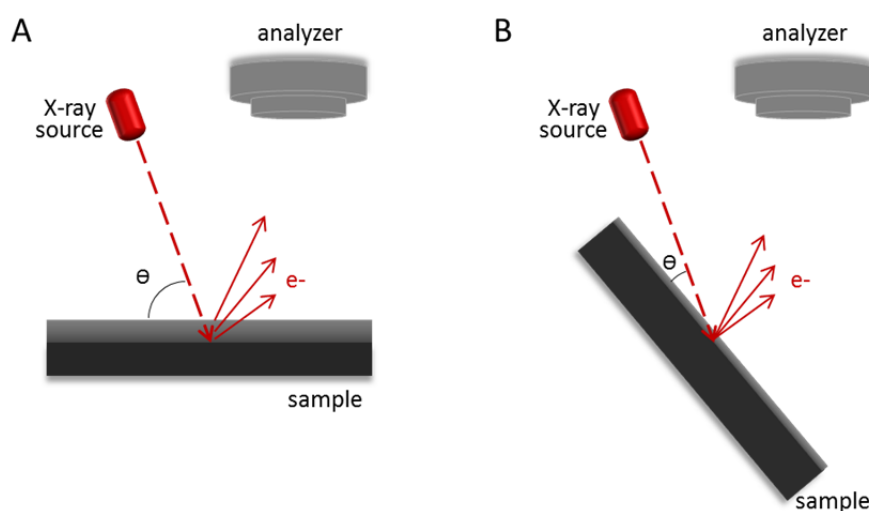


Figure 2.3.3-1. Angle-resolved XPS. X-ray incidence angle to the samples (take-off angle, θ) can be modified by sample tilt. (A) Regular θ of 70°. (B) Low θ of 20°.

Fourier transform infrared spectroscopy (FTIR)

FTIR measurements were done on a Nicolet Nexus 870 spectrometer in normal transmission mode using a deuterated triglycine sulfate (DTGS) KBr detector over the range of 400-4000 cm^{-1} at a 4 cm^{-1} resolution. All spectra were baseline-corrected.

Variable-angle spectroscopic ellipsometry

The thickness and optical properties of the polymerized films were analyzed on a J.A. Woollam M-2000 spectroscopic ellipsometer with a xenon light source. Ellipsometry measures a change in polarization as light reflects or transmits from the polymer. This change depends on the optical properties and thickness of the layer. Data were acquired at three angles (65°, 70°, and 75°) and 225 wavelengths, and the Cauchy-Urbach dispersion model was used to fit the data and obtain the thickness of the films.

This technique was also used to determine the swelling properties of the hydrogel layers. For this purpose a liquid cell (J.A. Woollam) was placed onto the M-2000 ellipsometer stage and film-coated substrates were secured in this cell. Measurements were performed before (air/solid interface) and after the cell was filled with PBS (solution/solid interface). The data from the dried film was fit with the Cauchy-Urbach model. Instead, two models were used to study the swollen films: the previously mentioned Cauchy-Urbach model, considering the wet film as a unique material with different properties than the dried film, and the effective medium approximation (EMA) model, widely described elsewhere⁴⁹, which assumes that the film is formed by two materials: the polymer matrix, with the same properties than the dried material, and water. Both models used water as ambient material. The required file (i.e., refractive index vs wavelength) for the polymer matrix was generated using the data obtained from the corresponding dried samples. The material file for water was obtained from J. A. Woollam.

Contact angle goniometry

The wettability of the films was evaluated by contact angle measurements, which were performed on a goniometer equipped with an automatic dispenser (Model 500, Ramé-Hart). The contact angle was determined by placing a drop of water on the surface and measuring the angle between the plane of the surface and the tangent to the drop at the point of contact with the substrate (measurement known as *sessile* drop). Dynamic contact angles measurements (advancing and receding) were performed, as the surfaces were usually in a non-equilibrium state. The advancing contact angle (θ_a) was measured by inserting the needle of the syringe into the drop, adding water in it, and measuring the maximum angle achieved (Figure 2.3.3-2 A). The receding contact angle (θ_r) was measured by removing water from the drop and measuring the minimum contact angle achieved (Figure 2.3.3-2 B).

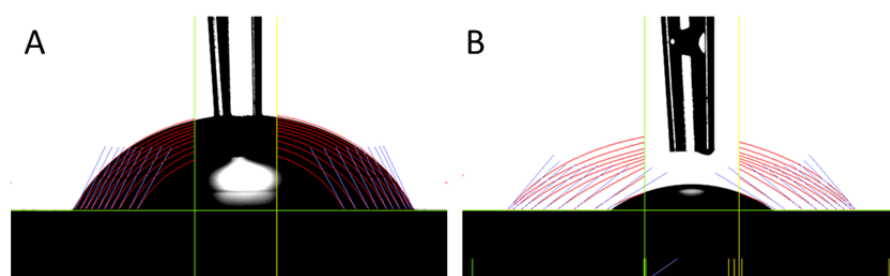


Figure 2.3.3-2. Dynamic contact angle scheme. (A) Advancing contact angle; the three phase line (air/water/solid) moves over and wets the surface. (B) Receding contact angle; the three phase line is withdrawn over the pre-hydrated surface.

Fluorescent microscopy

The reaction of PFM with a fluorescent label was verified under a Nikon Epi-Fluorescence microscope TE300 with FITC/GFP HyQ filter set (Nikon, NY).

Atomic force microscopy (AFM)

AFM images were acquired with two different microscopes from dried samples and films immersed in water. Nanoscope III Extended Multimode Atomic Force Microscope (Digital Instruments, Santa Barbara, CA), with a lateral resolution of 5 nm and vertical of 1 Å, was used for tapping mode analysis. Images were analyzed by Nanoscope III v4.22 software. Instead, XE-100 (PSIA Inc.) was used for non-contact mode analysis, with a lateral and vertical resolution of 0.15 nm and 0.05 nm, respectively. In this case, XEP and XEI software was used for data acquisition and image processing, respectively.

2.3.4. BIOLOGICAL ASSESSMENT**Cell growth and seeding**

Mouse embryonic fibroblasts (MEFs) were purchased from ATCC (cat# SCRC-1008) and expanded in 75 cm² flasks in growing medium, including 10 % fetal bovine serum (FBS) and 1 % (w/v) penicillin/streptomycin (Gibco) in Dulbecco's modified eagles medium (DMEM, Gibco). Cultures were maintained at 37 °C in a humidified incubator equilibrated with 5 % carbon dioxide.

Polymerized PFM films –modified or not with laminin-derived RYVVLPR peptide- were sterilized with ethanol 70 % and placed in 6-well plates and equilibrated in DMEM for 1 h in the tissue culture incubator at 37 °C. MEFs were harvested at approximately 80 % confluence using 0.05 %/0.02 % trypsin-EDTA and complete medium is used to inactivate the enzyme. Cell suspension was centrifuged at 60 x g for 5 min and suspended in DMEM to wash cells from remaining serum traces. After another centrifugation step and suspension in DMEM, cells were counted. Next, two sets of experiments were performed, in presence and absence of serum. For this purpose, the medium on the PFM samples was removed and fresh medium with or without serum was added to the corresponding samples. Cells were seeded at a concentration of 20,000 cells·cm⁻². Cultures were kept in the incubator for 2 and 12 h to study cell binding and morphology. Parallel cultures were carried out on the tissue culture plastic wells, as control.

Parallel subsets of experiments were carried out with human umbilical vein endothelial cells (HUVEC), acquired from Lonza (cat# CC-2519) and expanded in complete medium (EGM-2 Bullet kit, Lonza, cat# CC-3162).

Cell morphology evaluation

Afterwards, cultures were fixed with 2 % (w/v) paraformaldehyde for 1 h at room temperature, washed with PBS containing 0.1 % (w/v) Triton X-100 (30 min) and stained with 4',6-diamidino-2-phenylindole (DAPI, Molecular Probes) for nuclei and phalloidin–tetramethylrhodamine B isothiocyanate (Phalloidin-TRITC, Sigma) for cytoskeleton. Samples were covered with a volume of

Phalloidin (0.1 $\mu\text{g}/\text{ml}$ in PBS) for 25 min in the dark and then same volume of DAPI solution (0.1 $\mu\text{g}/\text{ml}$ in PBS) was added to the solution and left for 5 min more. Finally, samples were abundantly washed with PBS and visualized under Nikon fluorescence microscope.

2.4. RESULTS AND DISCUSSION

2.4.1. PFM POLYMERIZATION

Previous to the deposition of complex hydrogels incorporating pentafluorophenyl methacrylate (PFM), the polymerization of PFM alone –homopolymer- or crosslinked with ethylene glycol diacrylate (EGDA) –copolymer- was studied by iCVD.

iCVD of the pentafluorophenyl methacrylate homopolymer

Various conditions were tested for the deposition of the PFM polymer film (pPFM), which are detailed in Table 2.4.1-1. Basically, different PFM partial pressures were obtained, as a result of maintaining the PFM flow approximately constant (0.9 - 1.0 sccm) and changing both the total pressure and the partial pressure of the other species. The depositions were carried out at a filament temperature of 280 $^{\circ}\text{C}$ and a temperature stage of 30 $^{\circ}\text{C}$. It was observed that partial pressures of the monomer of 125 mTorr or higher led to the condensation of PFM on the substrate at that stage temperature. On the other hand, decreasing its partial pressure into the reactor involves slowing the deposition rate, as shown in samples P4 and P5. Thus, the concentration of PFM in the vapor phase must be low enough to avoid condensation, but high enough to provide an acceptable deposition rate. In this study, the maximum deposition rate achieved for the bare pPFM films was 27 $\text{nm}\cdot\text{min}^{-1}$, which is in the same order as the last results reported in the group using pulsed plasma (28 $\text{nm}\cdot\text{min}^{-1}$)³⁶ and much better than previous results (25 $\text{nm}\cdot\text{h}^{-1}$)³⁵.

Table 2.4.1-1. Experimental conditions for the bare PFM polymerization.

samples	flow / sccm			PFM partial pressure / mTorr	total pressure / mTorr	deposition rate / $\text{nm}\cdot\text{min}^{-1}$
	PFM	TBPO	N_2			
P1	0.93	0.23	0.93	178	400	--- ^a
P2	0.93	0.23	0.93	133	300	--- ^a
P3	1.0	1.0	0	125	250	--- ^a
P4	1.0	1.0	0	100	200	27
P5	0.93	0.23	0.93	89	200	21

^a Monomer condensation.

PFM was successfully polymerized by the iCVD technique with full retention of the pendant fluorinated phenyl group, as observed in Figure 2.4.1-1. The FTIR of the pPFM shows the

characteristic peaks of the fluorinated polymer. The strong absorption ranging from 1150 to 970 cm^{-1} correspond to the typical bands of the C-F stretching, and the two peaks observed at 1520 and 1475 cm^{-1} are related to the aromatic stretching vibrations. The peak around 1785 cm^{-1} indicates a carbonyl stretching absorption of a carboxylate ester and the weak absorption around 2950 cm^{-1} is in accordance with the alkane C-H stretching bands.

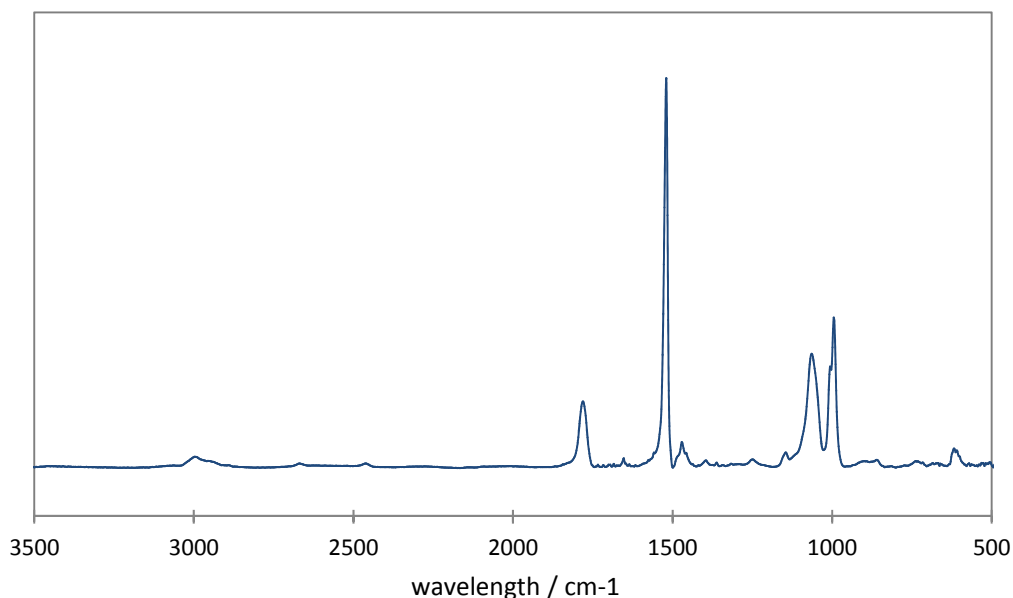


Figure 2.4.1-1. FTIR spectrum of PFM homopolymer film. It corresponds to the sample P4, with an approximate thickness of 400 nm.

XPS survey scan revealed the presence of carbon, oxygen and fluorine with a carbon-to-fluorine (C/F) ratio of 2.27, which is in good agreement with the theoretical ratio (2.00). Regarding the high-resolution XPS, the C1s signal was fitted on various oxygen-containing functionalities and on fluorine-containing functionalities.

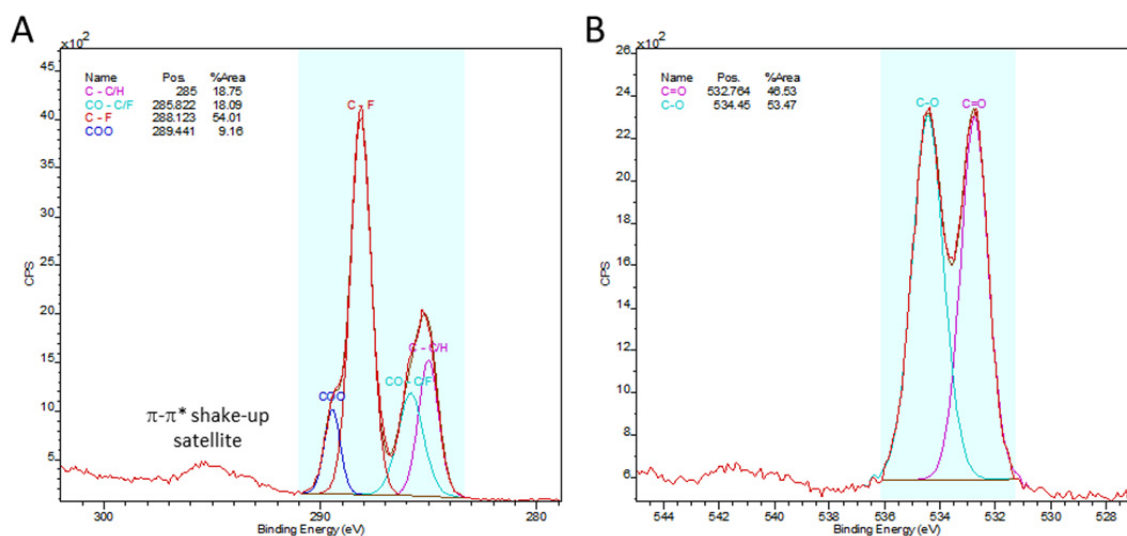
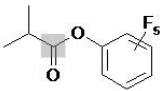
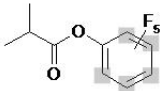
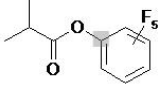
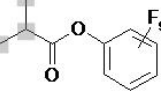


Figure 2.4.1-2. XPS high-resolution scan of the PFM homopolymer. Deconvolution of (A) C1s signal and (B) O1s signal, for sample P5. Spectra were corrected for sample charging, setting the hydrocarbon to 285.0 eV, and the position of the other centroids accordingly adjusted.

As indicated in Figure 2.4.1-2 A, the C1s core level show four carbon moieties, consistent with the chemical structure of the pentafluorophenyl methacrylate: the hydrocarbon (C-C/H), the α -ester carbon (C-COO), the ether carbon (CO-C/F) and the fluorinated carbon (C-F). Moreover, the scan clearly presents the $\pi \rightarrow \pi^*$ shake up satellite signal, which is characteristic of the aromatic structures and thus corroborates the ring retention.

Table 2.4.1-2 summarizes the area percentage for each peak and its binding energies, which show excellent agreement with data in the literature. The XPS high-resolution scan for O (Figure 2.4.1-2 B) is also in accordance with the PFM structure as it presents two O chemistries with the typical binding energies for a C=O* and a OC-O* peaks (532.76 and 534.45 eV, respectively)⁵⁰, and with nearly the same relative area, as it was expected. Consequently, the XPS corroborated the FTIR results and supported the retention of the monomer functionality.

Table 2.4.1-2. High-resolution XPS scan data of the iCVD pPFM filma.

origin	iCVD film		PFM reference ^a	
	binding energy / eV	% area	binding energy / eV	
COO		289.4	9.2	289.1
C-F		288.1	54.0	288.2
CO-C/F		285.8	18.1	286.2
C-C/H		285.0	18.7	285.0

^aThe literature values are from Francesch *et al.*³⁶

iCVD of the crosslinked pentafluorophenyl methacrylate

Although the linear PFM polymer is so hydrophobic that it does not dissolve in aqueous solutions, the possibility to crosslink the PFM films was proposed. Crosslinking would improve the mechanical properties of the films, making them more resistant under flows and some non-aqueous solvents. Moreover, by introducing a new compound in the film, PFM concentration on the surface would be lower, resulting in a less hydrophobic layer with improved interaction with water.

Ethylene glycol diacrylate (EGDA) was chosen as crosslinker, since the two esters groups make it rather hydrophilic. In addition, this divinyl compound is commonly used as crosslinking agent in solution-phase polymerization. Compared to ethylene glycol dimethacrylate (EGDMA), EGDA is only slightly more hydrophilic, but it has a higher vapor pressure that facilitates the methodology ($P_{EGDA}^V = 0.0939$ Torr and $P_{EGDMA}^V = 0.0121$ Torr at 25 °C -calculated values from SciFinder Scholar using Advanced Chemistry Development Software V9.04 for Solaris –© 1994-2007 ACD/Labs). Diethylene

glycol divinyl ether was also tested as crosslinker, as it contains two vinyl groups as well. However, since it is not an acrylate, it hardly reacted with PFM due to the different reactivity of the two double bonds. This behavior between acrylates and vinyl bonds of another nature had already been reported by Lou *et al.*⁵¹.

Hence, ethylene glycol diacrylate (EGDA) was introduced into the reactor together with PFM to synthesize crosslinked PFM films. Copolymer composition could be controlled by varying the gas feed ratio of the two monomers into the iCVD reactor, as demonstrated for copolymers of methyl α -chloroacrylate with methacrylic acid⁵² and for copolymers of hydroxyethyl methacrylate with ethylene glycol diacrylate⁴⁵. Nevertheless, the ratio on the surface does not correspond to the flow ratios on the vapor phase, but to the ratio of the adsorbed monomers. The amount of adsorbed monomer is, in turn, proportional to the ratio of the monomer pressure in the reactor to the monomer vapor pressure at the stage temperature (P_M/P_{sat}), as previously explained in the background (Section 2.1.7).

Two samples with different crosslinking densities were synthesized. As in the previous experiments, the temperatures of the filament and the stage were maintained at 280 and 30 °C, respectively, and the PFM and TBPO flows were kept constant while the EGDA flow was varied. A N₂ patch flow was also introduced into the chamber in order to keep the total flow rate constant (2.26 sccm) and consequently ensure the same residence time in both experiments (13 s). The details of the experimental conditions are indicated in Table 2.4.1-3.

Table 2.4.1-3. Experimental conditions for the PFM-co-EGDA polymerization.

samples	flow / sccm				partial pressure / mTorr		total pressure / mTorr
	PFM	EGDA	TBPO	N ₂	PFM	EGDA	
C1	0.78	0.28	0.20	1.00	104	37	300
C2	0.78	0.10	0.20	0.68	104	13	300

Figure 2.4.1-3 shows the detailed FTIR analysis in the carbonyl, aromatic, and fluorinated regions as the partial pressure of the EGDA was increased. Compared to the bare pPFM film (a), the aromatic (1520 cm^{-1}) and the C-F stretching vibrations ($1150\text{-}970\text{ cm}^{-1}$) decreased, when the EGDA concentration in the vapor phase increased (b, c). At the same time, a new carbonyl peak from EGDA (d) appeared a little bit shifted to the right (1730 cm^{-1}) compared to the PFM carboxyl (1770 cm^{-1}). Hence, it was possible to make crosslinked PFM films, which enhanced its properties when soaked in a solution.

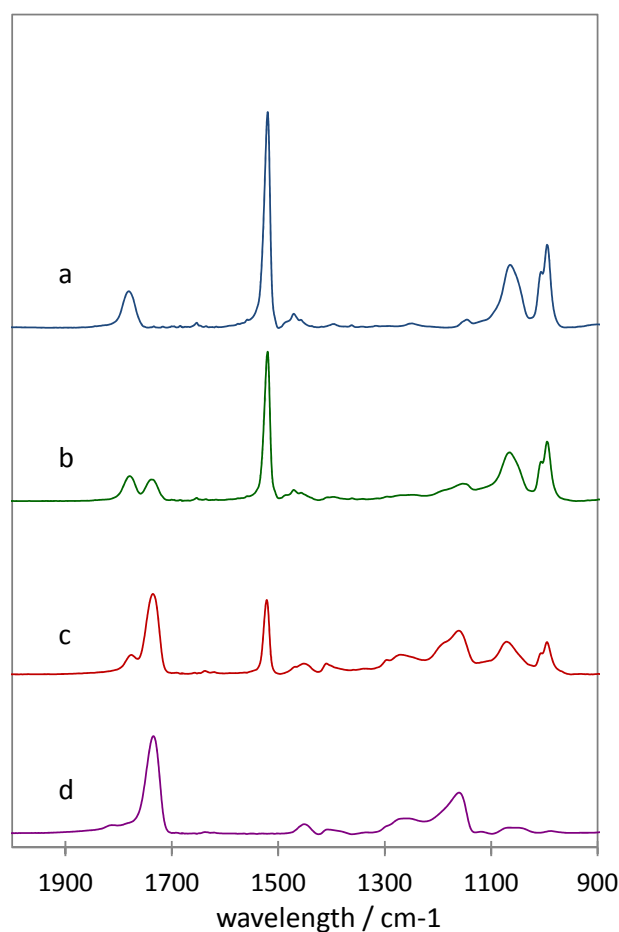


Figure 2.4.1-3. FTIR spectra of four polymer compositions. (a) Bare PFM polymer, (b) poly(PFM-co-EGDA) copolymer with EGDA to PFM ratio of 0.4, (c) the same copolymer with EGDA to PFM ratio of 3.6 and (d) bare EGDA polymer, all normalized for film thickness.

The ratio of the crosslinker to monomer in the deposited films gives an indication of the degree of crosslinking. These compositions can be calculated using the Beer-Lambert equation, which states that the absorbance of a mode (A) is proportional to the concentration of the moiety that is responsible for that particular mode. Then, Equation 2-1, which relates the C=O absorption for both monomers, could be used to determine the mentioned ratios, but it was necessary to assign precisely the corresponding absorption to each monomer ($A_{\text{C=O(EGDA)}}$ and $A_{\text{C=O(PFM)}}$). Moreover, this equation implies the assumption that the C=O bond absorption coefficient is the same in the PFM and EGDA components. Indeed, this supposition has been verified in other acrylic copolymers by comparing FTIR and XPS results⁴⁵. Therefore, the deconvolution of the carbonyl signal was necessary to obtain the two different C=O peaks and their associated areas. However, deconvolution of FTIR peak did not render precise results.

$$\frac{[\text{EGDA}]}{[\text{PFM}]} = \frac{A_{\text{C=O(EGDA)}}/2}{A_{\text{C=O(PFM)}}} \quad \text{Equation 2-1}$$

Therefore, another attempt was the subtraction of the absorption corresponding to the PFM carbonyl ($A_{\text{C=O(PFM)}}$) from the total C=O area (Equation 2-2). In turn, $A_{\text{C=O(PFM)}}$ was calculated by

association to a unique absorption of PFM, such as the aromatic stretching peak (C_{ar}). For this purpose, it was necessary to calculate a factor r_{PFM} , which is the ratio of the C=O absorbance to the C_{ar} absorbance for the bare PFM. This concept permitted to rewrite Equation 2-2 in Equation 2-3, as function of the total absorption of the carbonyl region ($A_{C=O(TOTAL)}$), the absorption of the aromatic bonds (A_{Car}) and the factor r_{PFM} that was calculated to be 0.34.

$$\frac{[EGDA]}{[PFM]} = \frac{(A_{C=O(TOTAL)} - A_{C=O(PFM)})/2}{A_{C=O(PFM)}} \quad \text{Equation 2-2}$$

$$\frac{[EGDA]}{[PFM]} = \frac{(A_{C=O(TOTAL)} - r_{PFM} \cdot A_{Car})/2}{r_{PFM} \cdot A_{Car}} \quad \text{Equation 2-3}$$

Therefore, it is possible to calculate the EGDA to PFM ratios in the films using FTIR data. With XPS high-resolution scan, it would be also possible to compute the composition from Equation 2-2, because XPS measures directly the atomic contributions. Nevertheless, it would require deconvolution of O peak into 5 different oxygen chemistries. Moreover, FTIR method is preferred, as the analysis is easier and the equipment is commonly more accessible.

2.4.2. PFM FUNCTIONALIZATION

As already mentioned, pentafluorophenyl methacrylate easily reacts with primary amines and, thus, it allows the attachment of many different biomolecules, whenever they have an accessible amine in their structure. In order to test different conditions for the reaction, the simple amine 1,6-hexyldiamine (Figure 2.4.2-1 A) was initially used as a reference molecule.

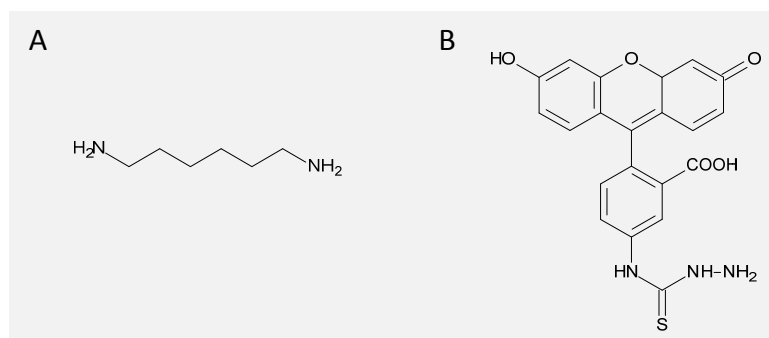


Figure 2.4.2-1 Chemical structure of the amine-containing molecules used as control. (A) 1,6-Diaminohexane. (B) Fluorescein-5-thiosemicarbazide (FTSC).

Test of different solvents and temperatures on reactivity of crosslinked PFM films

A pPFM film (EGDA / PFM = 1.3), approximately 200 nm thick, was incubated for different periods of time at room temperature and 60 °C with a 10 mM and 100 mM diamine solution in PBS (pH had to be readjusted at 7.8). The expected decrease of the intensities associated to the typical PFM stretching peaks in FTIR was really low, though noticeable especially at high concentrations, high temperatures and long times. A weak peak at 1665 cm^{-1} , corresponding to the newly formed amide

carbonyl, was also perceptible, meaning that PFM signals drop was not only due to the hydrolysis of the active ester (data not shown). Furthermore, the ellipsometric analysis showed no thickness loss over time. These two reasons ruled out the possibility that the diminution of the PFM intensity could be due to partial film dissolution. However, the reaction might be taking place only at the near surface, since the high hydrophobicity of PFM limited water diffusion into the bulk.

Both ethanol and N,N-dimethylformamide (DMF) were tried as alternative solvents to enhance the substitution reaction. Due to their lower polarity, they are supposed to interact better with the pPFM film and favor the fluorophenol leaving group solubility. Due to the risk of dissolution of the polymer when using hydrophobic solvents, these tests were run on crosslinked PFM samples. However, DMF partially dissolved the films and it was consequently dismissed. On the other hand, ethanol was thought to provide better results, as it is far less polar than water but still protic solvent, which typically enhances a nucleophilic attack. Then, the PFM films reactivity was proved in ethanol as well as in N,N-dimethylformamide/ethanol (10:90 v/v), both leading to a substantial degree of functionalization. Figure 2.4.2-2 showed the FTIR of a crosslinked PFM sample (EGDA/PFM = 1.3) before and after functionalization with a 100 mM diamine solution in ethanol at 60 °C for 12 h. The typical PFM peaks (the carbonyl at 1782 cm^{-1} , the aromatic carbon stretching peak at 1520 cm^{-1} and the C-F stretching region from 1150 to 970 cm^{-1}) are observed to substantially decrease, whereas a new peak in the carbonyl region appeared shifted to the right (1670 cm^{-1}), indicating the formation of an amide bond. The weak signal at 3420 cm^{-1} , characteristic of the N-H stretching, and the increase of the alkane C-H peak also corroborated the attachment of the 1,6-hexyldiamine.

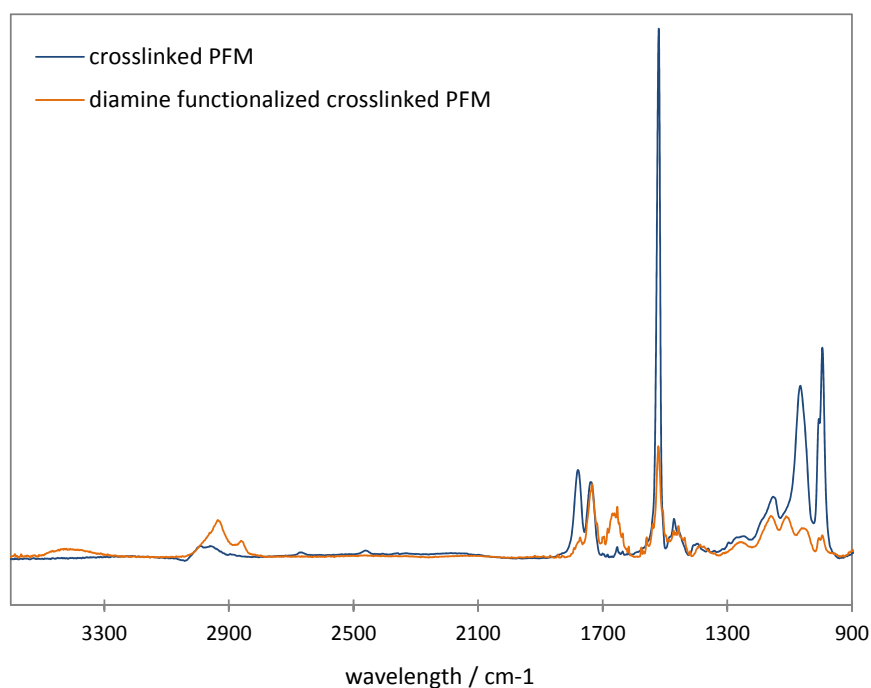


Figure 2.4.2-2. FTIR spectra of a crosslinked PFM film functionalization with diamine. It corresponds to a sample with an EGDA to PFM ratio of 1.3, before (blue) and after (orange) immersion in a 100 mM diamine solution in ethanol at 60 °C for 12 h.

Almost the same changes took place in DMF / ethanol (10:90 v/v), even at lower concentration of the reactant (10 mM 1,6-hexyldiamine), as shown in Figure 2.4.2-3. It was also observed that the degree of reaction dropped considerably when decreasing the temperature down to 37 °C. These differences were also corroborated by the contact angle results, since the film treated at 37 °C showed a contact angle (θ) value of 93°, whereas in the film treated at 60 °C contact angle was as low as 65° (the crosslinked sample had originally a θ value of 100°).

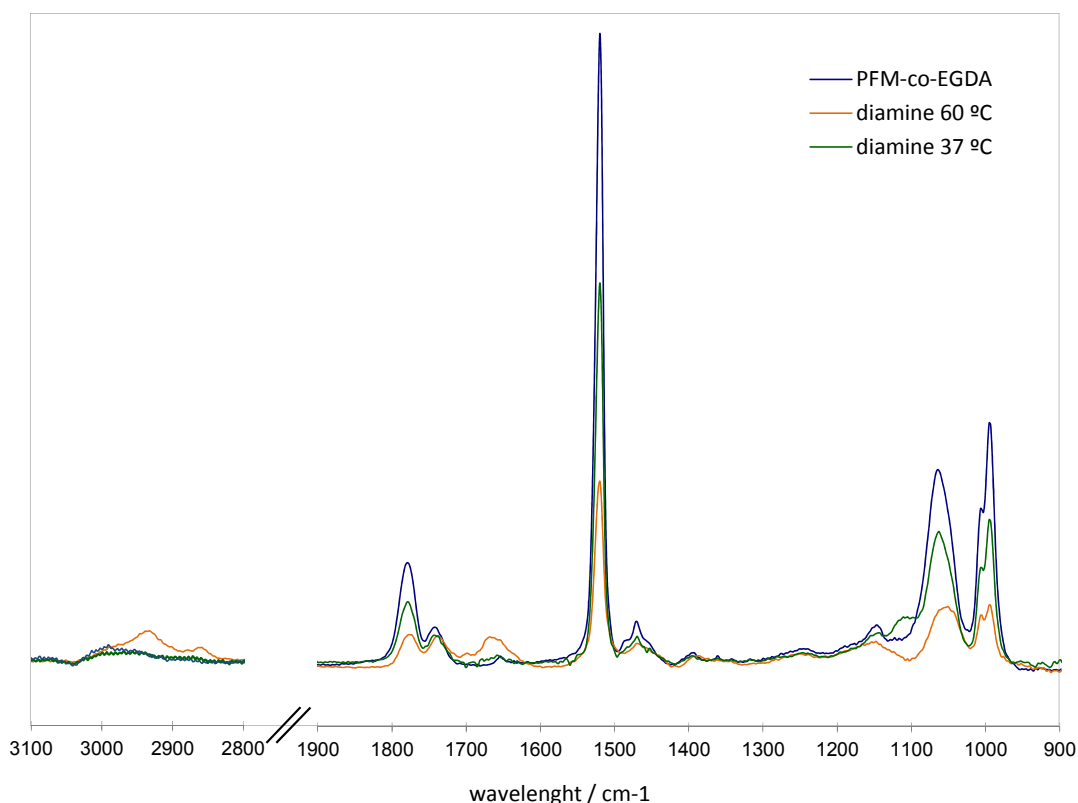


Figure 2.4.2-3. FTIR spectra of the diamine reaction with a crosslinked PFM film depending on the temperature. The PFM sample (EGDA / PFM = 1.3) was soaked in a 10 mM diamine solution in DMF / ethanol (10:90 v/v) for 12 h at 37 and 60 °C.

Crosslinked PFM film reactivity against peptides at mild conditions

The previous experiments showed how to optimize PFM film reactivity against amines. However, in order to couple biomolecules, it was decided to work in aqueous media to the detriment of the degree of reaction, since most biological ligands would lose their native structure in other solvents. Furthermore, only the molecules bound to the most outer PFM, facing the cells, are of real interest for the specific purpose of this work, and thus the efficiency of the reaction was set aside. The cell binding motif *N*-RYVVLPR-c was used as reference molecule to check the reactivity of the films against short peptides in mild conditions (1 mM peptide solution in PBS at 37 °C for 12 h).

As expected, FTIR data showed a very low global reactivity of the pPFM film, which was 100 nm thick. Therefore, XPS survey scan was performed to get information of the first 4 to 10 nm. Table 2.4.2-1 presents the elemental composition for an untreated PFM sample (T1), a control sample immersed in

PBS (T2) and a sample treated with peptide (T3), along with their contact angle values. After the reaction with peptide, the N percentage was observed to increase at the same time that the F content substantially decreased, indicating both the loss of the fluorinated labile group and the appearance of nitrogenated moieties. The attachment of the peptide was also consistent with the considerable C content increase and the slight O increase. Figure 2.4.2-4 shows the XPS profiles of the carbon, fluorine and nitrogen signals. In PBS without peptide (sample T2), the F percentage also diminished but in a smaller extent than in the peptide-modified film. This effect is due to the hydrolysis of the active ester, which could be especially significant during extended immersions, as previously studied³⁶. However, that work also stated that the reaction with aqueous buffer was much slower than that with primary amines such that the reaction between the amine and the ester groups will always dominate reaction pathways under solvent environment. This statement is also confirmed in the present work, since the peptide effect on the atomic percentages is clearly more important than the hydrolysis effect. Finally, it should be mentioned that the XPS results also showed a slight increase in C, O and N contents in PBS-treated samples, which could be due to trace air or, more probably, to some kind of contamination. In any case, the differences between the values are significant enough to consider that there was peptide attachment, beyond the water effect.

Table 2.4.2-1. XPS survey scan comparison of the peptide modified and the non-modified PFM.

samples	XPS atomic percentages				θ_A
	C	O	F	N	
T1	63.50	10.19	26.31	0.00	100
T2	65.53	11.81	21.71	0.94	86
T3	76.27	12.11	8.60	2.91	59

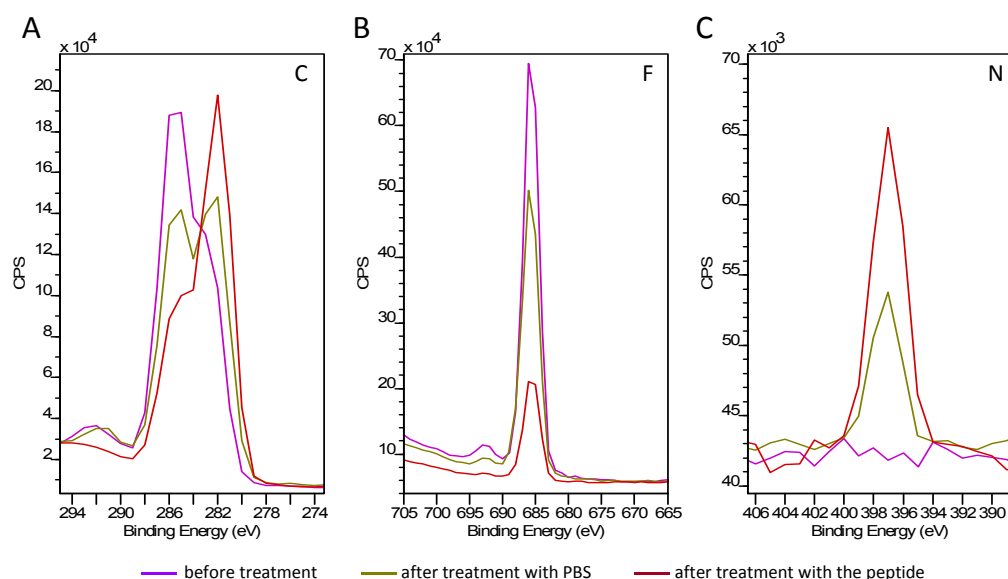


Figure 2.4.2-4. XPS survey scan of the coupling of N-RYVVLPR-C peptide to PFM. The graphs showed (A) carbon, (B) fluorine and (C) nitrogen signals for the same PFM sample (EGDA / PFM = 0.11). The purple line corresponds to the sample before treatment, the red line to the sample soaked in 1 mM peptide solution in PBS and the green line to the sample soaked only in PBS under the same conditions.

Finally, water contact angles were examined on the three samples (Table 2.4.2-1), as they are expected to be different before and after each treatment. As estimated, the surface became more hydrophilic after immersing the PFM film in water, changing its contact angle from 100 to 86. This result is in agreement with the partial hydrolysis of the PFM on the surface. But the surface hydrophilicity changed to a great extent when treated with peptide, achieving a contact angle value of 59, which ensures that the modification took place.

Finally, the fluorescent amine FTSC (see Figure 2.4.2-1 B) was used to easily check the success of the reaction by fluorescence microscopy. Figure 2.4.2-5 shows the fluorescence micrograph of one sample of EGDA polymer and another of crosslinked PFM, which had been treated with a 0.5 mM FTSC solution also in ethanol at 60 °C for 12 h. The green surface confirmed the binding of the fluorescent marker to the PFM and no sign of adsorption on the film with no PFM available. The higher sensitivity of this method allows the detection of the coupling even when it happens only in the first PFM layers, as long as the aminated reagent contains a fluorescent label. Therefore, this strategy avoids constant use of a complex technique such as XPS.

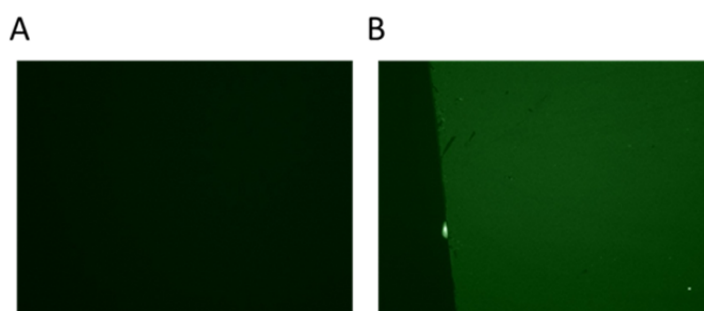


Figure 2.4.2-5. Immobilization of fluorescein-5-thiosemicarbazide. The fluorescent amine was incubated with (A) a pEGDA film and (B) a p(PFM-co-EGDA) film.

2.4.3. HEMA HYDROGELS WITH PFM

iCVD polymerization of the ternary system HEMA-co-EGDA-co-PFM

Once the synthesis of PFM films by iCVD was proven, the copolymerization of a HEMA hydrogel with PFM monomers was tried. As a result, a platform combining materials with different viscoelastic properties and with the possibility to link various biomolecules might be produced.

In order to polymerize this ternary system, PFM was heated and introduced into the reactor chamber together with HEMA and EGDA monomers. Figure 2.4.3-1 proves that all three components are polymerized together, as the aromatic stretching peak appeared in the terpolymer (1520 cm^{-1}), indicating the presence of PFM among the HEMA and EGDA characteristic signals (O-H stretching at $3700\text{-}3050\text{ cm}^{-1}$, C-H stretching at $3050\text{-}2700\text{ cm}^{-1}$, C=O stretching at $1750\text{-}1690\text{ cm}^{-1}$, C-H bending $1500\text{-}1350\text{ cm}^{-1}$ and C-O stretching at $1300\text{-}1200\text{ cm}^{-1}$). In addition, the XPS measurements revealed a fluorine percentage that oscillates between 2.15 and 2.79 % and no signal of N was observed.

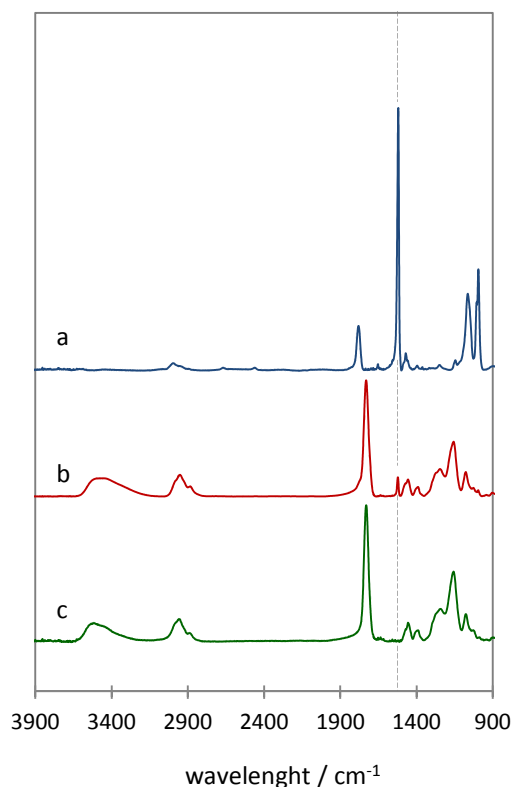


Figure 2.4.3-1. FTIR spectra comparison showing the PFM incorporation into the hydrogel. FTIR spectra of (a) bare PFM, (b) HEMA-co-EGDA-co-PFM terpolymer and (c) HEMA-co-EGDA hydrogel. In the terpolymer (b), the characteristic aromatic stretching vibration of PFM at 1525 cm^{-1} is clearly distinguished among the HEMA and EGDA signals.

A series of PFM containing hydrogels with different degrees of crosslinking was prepared. The flow rates of HEMA (0.30 sccm), PFM (0.04 sccm) and TBPO (0.15 sccm) were kept constant, while flow rate of EGDA was varied. A patch flow of nitrogen was also used to maintain the total flow rate at 2 sccm and the reactor pressure was kept at 200 mTorr. Table 2.4.3-1 summarizes the experimental conditions that ensured a constant residence time in the reactor of 10 s for all the experiments. The thickness of the different samples was approximately 600 nm.

Table 2.4.3-1. Experimental conditions of HEMA-co-EGDA-co-PFM polymerization.

sample	flow rates / sccm					partial pressure / mTorr		
	HEMA	EGDA	PFM	TBPO	N ₂	HEMA	EGDA	PFM
HE4P	0.30	0.11	0.04	0.15	1.40	38	14	5
HE2P	0.30	0.08	0.04	0.15	1.45	38	10	5
HE1P	0.30	0.06	0.04	0.15	1.47	38	8	5

Using the same approximation as in the PFM-co-EGDA films for the calculation of the degree of crosslinking, it was possible to obtain the PFM to HEMA as well as the EGDA to HEMA ratios in that ternary system. In this case, another factor for HEMA was needed (r_{HEMA}), apart from the PFM factor ($r_{\text{PFM}} = 0.34$). As r_{PFM} related the absorbance of the carbonyl to the aromatic carbons, r_{HEMA} is the ratio

of the C=O absorbance to the OH one for HEMA, which was calculated to be 0.53. Therefore, the C=O absorbance of PFM and HEMA can be rewritten as function of unique absorptions of these molecules: aromatic carbon and hydroxyl group, respectively. Equation 2-4 relates the C=O absorbance ascribed to the PFM monomer with the C=O signal coming from HEMA to obtain the PFM to HEMA ratio. For all the samples this ratio was maintained constant at a value of 0.03.

$$\frac{[\text{PFM}]}{[\text{HEMA}]} = \frac{A_{\text{C=O(PFM)}}}{A_{\text{C=O(HEMA)}}} = \frac{r_{\text{PFM}} \cdot A_{\text{Car}}}{r_{\text{HEMA}} \cdot A_{\text{OH}}} \quad \text{Equation 2-4}$$

In the same way, Equation 2-5 expresses the EGDA to HEMA ratio in a modification of the previously discussed Equation 2-1 for PFM-co-EGDA. In this case, all three monomers are incorporated in the expression that serves as an indicator of the degree of crosslinking in the terpolymer.

$$\frac{[\text{EGDA}]}{[\text{HEMA}]} = \frac{A_{\text{C=O(EGDA)}}}{A_{\text{C=O(HEMA)}}} = \frac{(A_{\text{C=O(TOTAL)}} - r_{\text{PFM}} \cdot A_{\text{Car}} - r_{\text{HEMA}} \cdot A_{\text{OH}})/2}{r_{\text{HEMA}} \cdot A_{\text{OH}}} \quad \text{Equation 2-5}$$

Figure 2.4.3-2 A shows the EGDA/HEMA ratio in the film as a function of the EGDA partial pressure. As it could be anticipated, the incorporation of EGDA increased at higher EGDA partial pressure, due to a rise of the adsorbed species concentration on the surface.

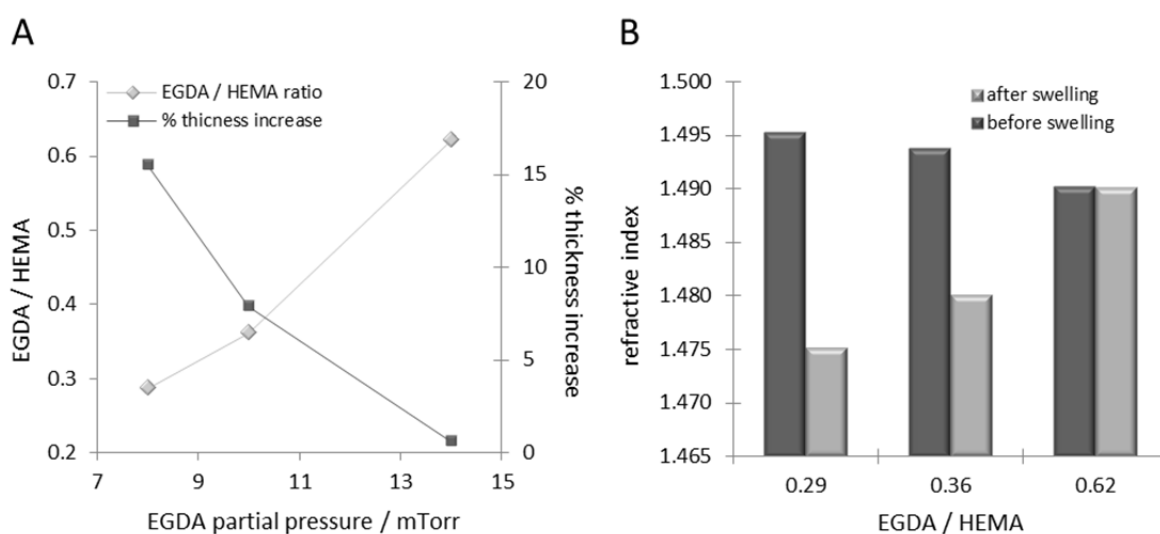


Figure 2.4.3-2. Crosslinking degree and swelling properties of HEMA-co-EGDA-co-PFM films. (A) Changes in the degree of crosslinking and the film thickness as function of the EGDA partial pressure. (B) Refractive index of the samples with different EGDA concentration before and after swelling in PBS.

The same graph also reports the corresponding swelling behavior of the samples as function of the EGDA partial pressure. The degree of swelling was calculated by ellipsometry as the difference in the film thickness before and after soaking in PBS. Once again, the plot is consistent with the expected results, as the crosslink density limits the film's ability to swell. Basically, higher amounts of crosslinker lead to lower incorporation of water in the hydrogel as the structure is more tightly held. In all the runs performed the thickness increase was quite low (0.6 - 15.5 %), therefore the concentration of EGDA is considered rather high. In the case of the sample with less crosslinker

(EGDA / HEMA = 0.29), the thickness increase was 15.5 %, which is rather lower than in the linear polymer, which was reported to swell up to a 55 % of thickness increase, corresponding to a 35 % (v/v) of water absorption⁴⁵. Therefore, new films with lower EGDA content would lead to a higher range of swelling degrees, between 15 % and 55 %. The HEMA homopolymer, though, was discarded because the film must be soaked for a long time in water and in these conditions pHEMA was observed to partially dissolve. It was thus decided to work with EGDA to HEMA ratios lower than 0.29 for subsequent experiments, excluding the HEMA homopolymer.

The refractive indexes (η) of the previous samples were also obtained from the ellipsometric measurements and model fitting. This property is a measure of the amount of impedance that a particular material has to the propagation of light and, consequently, its value reflects the changes in the chemical composition of a material, which make it an interesting parameter to consider. Figure 2.4.3-2 B depicts the refractive index values for the three differently crosslinked hydrogels containing PFM, before and after soaking. On one hand, the refractive index was observed to slightly decrease with increasing the amount of EGDA in the dry film, indicating small variations in the chemical composition. On the other hand, the water uptake radically modified the refractive index, which strongly decreased with reducing the EGDA component. The reason for this behavior is that a lower crosslink degree involves the retention of higher amount of water in the hydrogel structure. This change in the chemical composition is reflected in a consequent reduction of the refractive index, because water has a much lower refractive index ($\eta_{\text{H}_2\text{O}} = 1.33$) than the polymer. In the particular case of the less crosslinked sample, the refractive index has a value of 1.488 that decreases to 1.466 when swollen.

Functionalization of the ternary system HEMA-co-EGDA-co-PFM

In order to prove the reactivity of the PFM embedded into the hydrogel, the films were soaked in 1,6-hexyldiamine in N,N-dimethylformamide / ethanol (10:90 v/v). The advancing contact angles of the sample before and after the treatment provide evidence of the success of the reaction (Figure 2.4.3-3). The advancing angles are representative of the hydrophobic character of the films. Indeed, the amine-modified film lost hydrophobicity by substitution of the highly hydrophobic moiety (pentafluorophenyl) for the more hydrophilic diamine molecule. Therefore, contact angle dropped from 65.5 to 57.4. In contrast, the receding angles respond to the hydrophilic components of the samples (the hydrogel), which is constant in both samples. For this reason, receding angle follows the same behavior for the modified and the non-modified samples. This differential behavior between advancing and receding contact angle is known as contact angle hysteresis and it is more extensively explained in the next section.

If the solvent is exchanged for PBS, the reaction is noticeable at the near surface even after 5 h at room temperature, as proved by the appearance of N in the XPS survey scan (Table 2.4.3-2). Moreover, nitrogen increase is consistent with fluorine decrease. Nevertheless, fluorine is still present on the near surface after 5 hour-reaction.

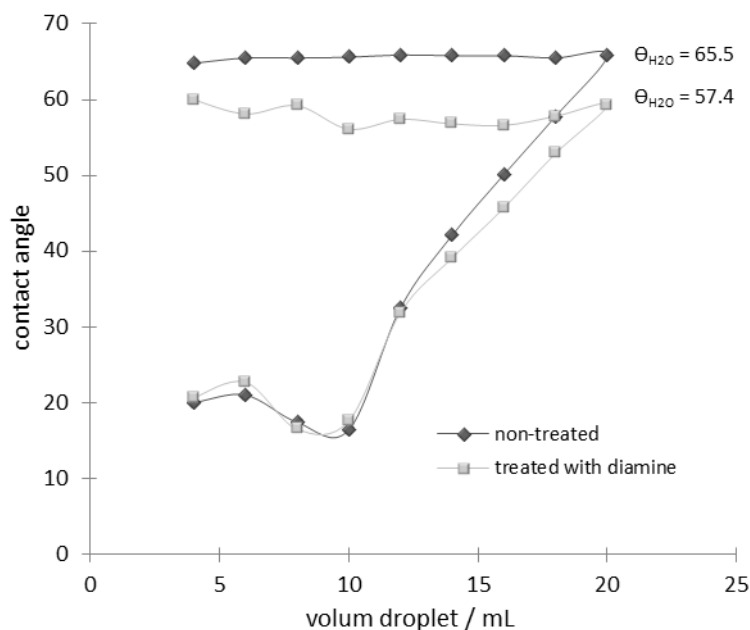


Figure 2.4.3-3. Advancing and receding contact angle of the hydrogel with PFM before and after treated with diamine. The advancing angles showed the different hydrophobicity.

Table 2.4.3-2. XPS survey scan before and after diamine reaction in PBS for the terpolymer.

samples	XPS atomic percentages	
	F	N
before treatment	2.77	0.00
after treatment	1.00	0.74

iCVD polymerization of a 2-layer film and dry characterization

From the previously discussed hydrogels, nanofilms with different swelling behaviors and with reactive sites throughout the hydrogel were achieved. However, posterior reactions in aqueous media were not as effective as expected, probably due to a low PFM concentration. Working in the same direction to obtain functionalized surfaces with tailored mechanical properties, a new design was suggested to restructure these films. Since increasing the PFM concentration in the hydrogels would lead to a more hydrophobic hydrogel (limiting its swelling capacity), a 2-layer approach was proposed to optimize its reactivity (HEMA-co-EGDA / PFM). Therefore, instead of synthesizing a homogeneous coating, the new strategy lie in a first polymerization of the HEMA-co-EGDA hydrogel and a consecutive deposition of PFM on top (Figure 2.4.3-4). Thus, the hydrogel bulk confers the viscoelastic properties to the film and the higher concentration of the active molecules at the surface favors the reaction with the biomolecules, which in addition will be exclusively located on the near surface. Moreover, this approach makes possible to reduce, to a large extent, the amount of needed PFM and thus to cut the cost of the process.

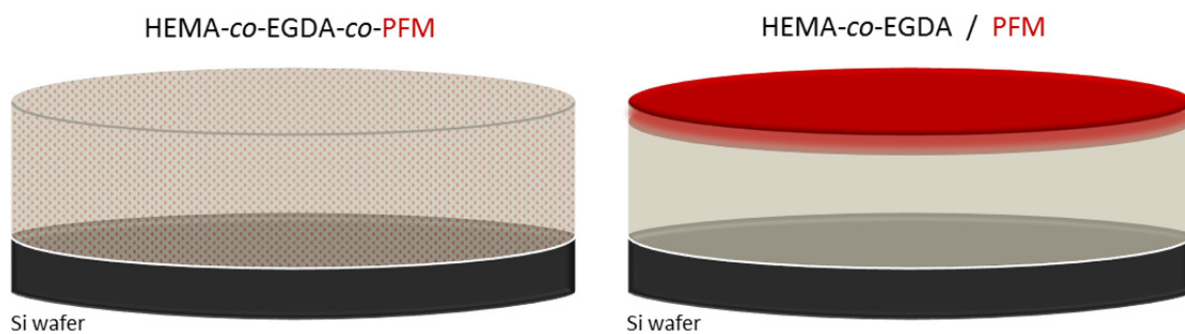


Figure 2.4.3-4. Scheme of the two approaches studied for the soft surfaces. PFM located throughout the whole hydrogel (left drawing) and on the surface (right).

In order to synthesize this system, the HEMA-co-EGDA hydrogel was initially polymerized until the interferometer indicated the desired thickness. Afterwards, the HEMA valve was closed and simultaneously the PFM valve was opened (in some cases EGDA was also polymerized with PFM). Meanwhile, the initiator and nitrogen flows and the filament heating kept running. As the new vapor mixture flowed through the filament, the thermal conductivity and the specific heat changed and, thus, the heat loss was also modified. As a result, the temperature of the filament underwent a change, so that the supplied power had to be readjusted. Once the system stabilizes, PFM was let polymerize until the desired thickness was reached.

This strategy allowed forming a two-layer film with tunable thicknesses: a hydrogel bulk covalently linked to a PFM polymer. Different samples were synthesized varying the PFM layer thickness in an approximate range from few nanometers to hundreds. Ellipsometric analysis was tried in all the samples in order to independently characterize the two layers. For this purpose, a two-layer model was used to fit the data, although the results were not always as consistent as expected, especially as the PFM layer was thinner. Table 2.4.3-3 shows the results of the fit for three samples, comparing the one-layer (considering the film as a whole polymer) and the two-layer models. The mean square error (MSE) was used to determine the best fit, which in general corresponds to the most complex model (two-layer).

Both the HP1 and HP2 samples presented a lower MSE when two layers were fitted. Furthermore, the addition of the thickness values of the hydrogel and the PFM is consistent with the total thickness obtained with the one-layer model. Regarding the index of refraction, the hydrogel layer always presented a higher value than PFM, since HEMA-co-EGDA usually showed values in the range of 1.48 and 1.51, while the index of refraction of pPFM was calculated to be lower, around 1.46-1.47 (data obtained from ellipsometric analysis). Obviously, the resulting index of refraction may substantially differ due to the presence of the crosslinker EGDA. In the third sample (HP3) the correlation between the experimental and the calculated data was not so good, as indicated by the MSE value and especially by the error values associated to the thicknesses of each layer. This fit proved that it is hard to effectively distinguish the two layers when the PFM layer is too thin.

Table 2.4.3-3. Spectroscopic ellipsometry analysis of the hydrogels with a PFM layer.

samples	parameters	one-layer model	two-layer model	
HP1	MSE	17.53	10.86	
	thickness / nm	270 ± 0.9	HEMA	102 ± 3
			PFM	170 ± 3
HP2	index of refraction	1.4884	HEMA	1.5251
			PFM	1.4493
	MSE	8.068	3.216	
HP3	thickness / nm	197 ± 0.5	HEMA	128 ± 4
			PFM	63 ± 4
	index of refraction	1.4810	HEMA	1.5137
HP3			PFM	1.4850
	MSE	14.67	14.74	
	thickness / nm	120 ± 0.4	HEMA	100 ± 34
HP3			PFM	20 ± 34
	index of refraction	1.4989	HEMA	1.4996
			PFM	1.4950

Unlike the ternary hydrogels (HEMA-co-EGDA-co-PFM) that presented a percentage of fluorine below 3 %, the two-layer approach made possible fluorine concentrations on the surface from 0 to nearly 30 %, the last one corresponding to the bare pPFM. As shown in Table 2.4.3-4, the atomic percentages of XPS of the hydrogel with PFM agreed with the bare pPFM, indicating that it is possible to create a compact PFM layer on top of the hydrogel.

Table 2.4.3-4. XPS survey scan of PFM polymer and hydrogel/PFM samples.

samples	XPS atomic percentages			
	C	O	F	F / C
pPFM	63.31	8.78	27.91	0.44
hydrogel / pPFM	63.21	9.45	27.34	0.43

However, these percentages were not always reached. On the contrary, the XPS data usually presented much lower F / C ratios, which meant a lower PFM concentration on the near surface and thus indicated a blend between the deposited hydrogel and the subsequent pPFM growing layer. This hypothesis was also confirmed by contact angle measurements, since it was observed that the contact angle increased with increasing the fluorine to carbon ratio from XPS (Figure 2.4.3-5). The contact angle value ranged from 58, for a HEMA-co-EGDA hydrogel with no PFM (with an EGDA/HEMA ratio of 0.14), to 96, for a hydrogel with enough PFM on top to get a F / C of 0.42, nearly equal to the bare pPFM. A simple linear regression analysis could explain the relationship between the contact angle results and the F / C ratios on the surface, with a coefficient of determination (R^2) of 0.9832.

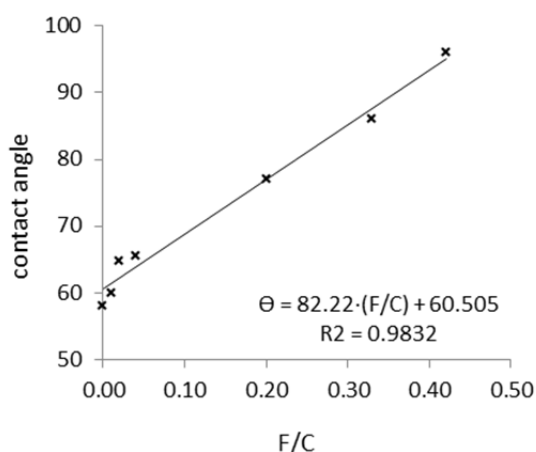


Figure 2.4.3-5. Contact angle measurements of the hydrogel / PFM films vs surface F / C ratio. Sessile contact angle of various hydrogels are plotted vs the F / C ratio on the surface obtained by XPS.

In order to study more accurately the first nanometers of the hydrogels with PFM, angle-resolved XPS (ARXPS) was performed at 20° and 90°. The variation of the take-off angle allows studying the elemental composition depending on the depth in a non-destructive way. When the angle is 90°, the X-ray is perpendicular to the surface, so that goes deeper into the film than at an angle of 20° from the surface. Hence, the F / C atomic ratios could be determined as function of the sampling depth for three hydrogels with different PFM content and for a PFM-co-EGDA copolymer. Equation 2-6 was used to approximately calculate the sampling depths, which are function of the take-off angle (θ) and the photoelectron escape depth (λ), which was estimated by Schmith *et al.* for hydrophobic polymeric coatings containing fluorine^{44,53}.

$$\text{depth} = 3 \cdot \lambda \cdot \sin(\theta) \quad \text{Equation 2-6}$$

For all the hydrogels with PFM, the F / C ratio in the first 8 nm (take-off angle of 90°) was higher than F / C that would correspond to the whole film calculated from the FTIR analysis. When only the first 2.7 nm were analyzed (take-off angle of 20°), the F / C was observed to increase even more (Table 2.4.3-5)

Table 2.4.3-5. Angle-resolved XPS of hydrogels with PFM.

sample	% PFM ^a	F / C		XPS sampling depth / nm
		bulk ^a	surface	
HEMA-co-EGDA / PFM	0.1	0.003	0.15	2.7
			0.08	8.0
	0.6	0.009	0.38	2.7
			0.26	8.0
20	0.259	0.47	2.7	
		0.43	8.0	
PFM-co-EGDA	45	0.504	0.43	2.7
			0.42	8.0

^a Values from FTIR analysis.

Therefore, these results revealed an enrichment of fluorinated units towards the surface and thus the formation of a PFM graded layer. As a control, ARXPS was also performed on a copolymer of PFM and EGDA with an EGDA / PFM ratio of 0.11, since certain degree of segregation of fluorinated monomers had also been previously reported for simple iCVD copolymers of glycidyl methacrylate with 2,2,3,3,4,4,5,5,6,6,7,7-dodecafluoroheptyl acrylate⁴⁴. In the control, however, a difference of the F / C ratio as function of depth was hardly appreciated, indicating that this phenomenon is typical of the two-layer film.

Behavior of the 2-layer films in aqueous medium

A lot of information regarding the behavior in water of these samples may be extracted from the contact angle analysis, especially from the advancing and receding mode. In these measurements a difference between the advancing and the receding angles is usually observed and corresponds to an effect known as contact angle hysteresis⁵⁴⁻⁵⁶. This phenomenon had been previously observed on different gel samples and was attributed to a change of the surface configuration due to a surface equilibration with the medium^{45,54,55,57}. Factors such as the heterogeneity, the roughness and the mobility of the polymer films may affect this surface behavior⁵⁸. Initially, the surface is in equilibrium with air, so that the hydrophobic domains (in the case of our samples, the PFM and the methyl groups of HEMA) are basically exposed and, consequently, the advancing contact angle is high. Once the surface is in contact with water, it establishes a new equilibrium with the aqueous medium, which involves a chain reorientation^{59,60}. Now mainly the hydrophilic moieties, like the hydroxyl groups of HEMA for the films here synthesized, are in contact with water. This more hydrophilic surface configuration holds back the water, which causes a flattening of the droplet and thus a decrease in the receding contact angle. A schematic representation of the structure of the polymer film interface both with air and water is drawn in Figure 2.4.3-6. Actually, similar structures have been proposed before for poly(ethylene glycol) with fluoroalkyl endgroups⁶⁰.

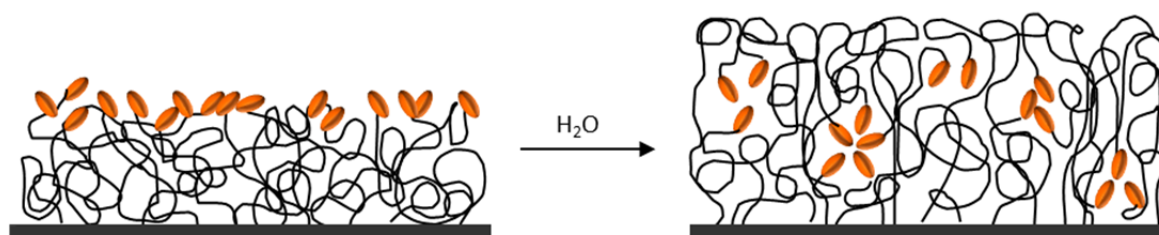


Figure 2.4.3-6. Schematic representation of the polymer brushes in different media. The image at the left shows the configuration of the polymer exposed to air, with the pentafluorophenyl groups (in orange) on the surface. Once equilibrated in water, the polymer structure changes to the one at the right, where the hydrophobic moieties bury themselves and the outer surface of the film is exclusively HEMA (black lines).

The advancing and the receding contact angles as function of the droplet volume for a bare hydrogel and a hydrogel with a PFM layer on top are depicted in Figure 2.4.3-7. As shown in the plot, the advancing angles did not change with droplet volume, because as the droplet size increased, there was always a part of the droplet in contact with surface that had not been wet yet and thus had not suffered chain reorientation. On the other hand, the receding angles decreased, because the contact

angle was kept constant while the drop volume decreased, therefore the droplet flattens until the true contact angle is reached. As the advancing angles are sensitive to the hydrophobic domains, the hydrogel with PFM on top presented a higher advancing angle than the bare hydrogel. In particular, a mean value of 86 was obtained (F / C ratio about 0.33), while the absence of PFM involved a contact angle of 55. But as both samples share the same hydrophilic domains (HEMA-co-EGDA with same crosslinking density of 0.14), the receding angle finally reaches the same value ($\theta_{\text{H}_2\text{O}} = 22^\circ - 24^\circ$). Therefore, for hydrogels with the same crosslinking densities, the degree of hysteresis will be different depending on the amount of PFM on the surface.

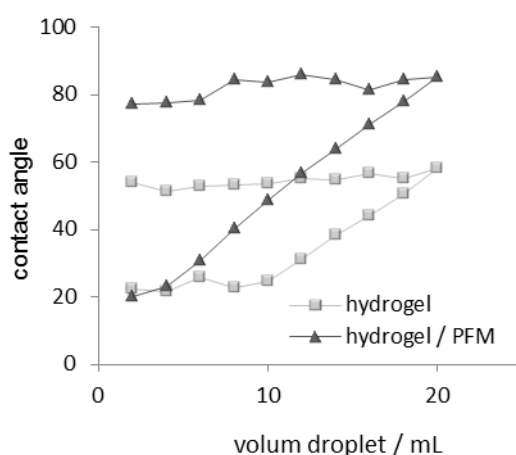


Figure 2.4.3-7. Contact angle hysteresis of hydrogel / PFM and bare hydrogel films. Advancing and receding contact angle as function of the droplet volume of a HEMA-co-EGDA hydrogel and a HEMA-co-EGDA / PFM hydrogel with F / C = 0.33.

Initially, a main concern regarding the application of the two-layer approach was the possible inability of the hydrogel to swell, caused by the limitation of water to diffuse through the highly hydrophobic surface. However, the fact that PFM forms a graded layer might help diffusion and, thus, films could still be suitable for the proposed applications.

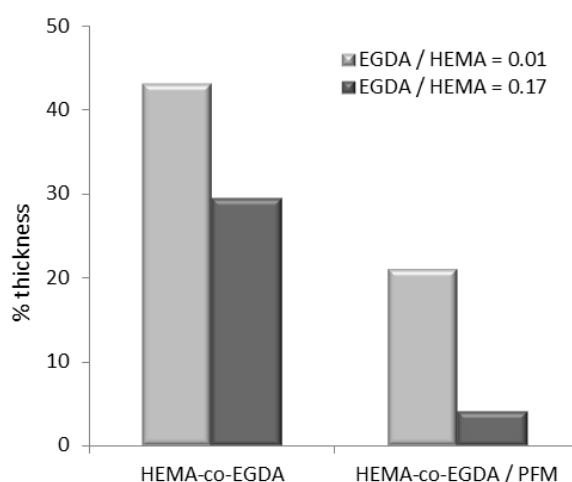


Figure 2.4.3-8. Decrease of the swelling ability in water for hydrogels with PFM on surface, compared to the bare hydrogels. The drop is corroborated for two samples with different crosslinking degrees, EGDA / HEMA = 0.01 and 0.17.

Indeed, ellipsometry measurements showed that hydrogels with PFM swelled (Figure 2.4.3-8). However, the increase of thickness shown in the hydrogels with PFM was lower than in the bare hydrogels with the same crosslinking density, indicating a clear dependence of the degree of swelling on the surface percentage of fluorine.

This effect was studied in more detail by correlating thickness increase in water with the fluorine content. The resulting graph pointed out that the swelling ability decreased with increasing the amount of fluorine on the surfaces (Figure 2.4.3-9 A). Unfortunately, values are not fully comparable, since the crosslinking densities for the three hydrogels are not the same and this factor plays an essential role in the swelling capability. In particular, the film with a fluorine amount of 5.43 % was synthesized with an EGDA / HEMA ratio of 0.13, whereas the other two have a degree of crosslinking of 0.17. For bare hydrogels, these crosslinking densities would imply an estimated thickness increase of 33 % and 30 %, respectively. These values were obtained after synthesis and characterization of hydrogel films with distinct crosslinking degrees. Thickness increase was found to follow a linear tendency in the range from 0.01 to 0.2 of EGDA / HEMA ratios, which permitted to estimate the swelling ability of hydrogels (Figure 2.4.3-9 B). Beyond these limits, the relation adopted a hyperbolic behavior⁴⁵. Based on these results, the differences in thickness increase depending on PFM content override the variation (3 %) due to the distinct crosslinking degree. Therefore, the trend followed by the swelling ability as function of the fluorine amount was confirmed.

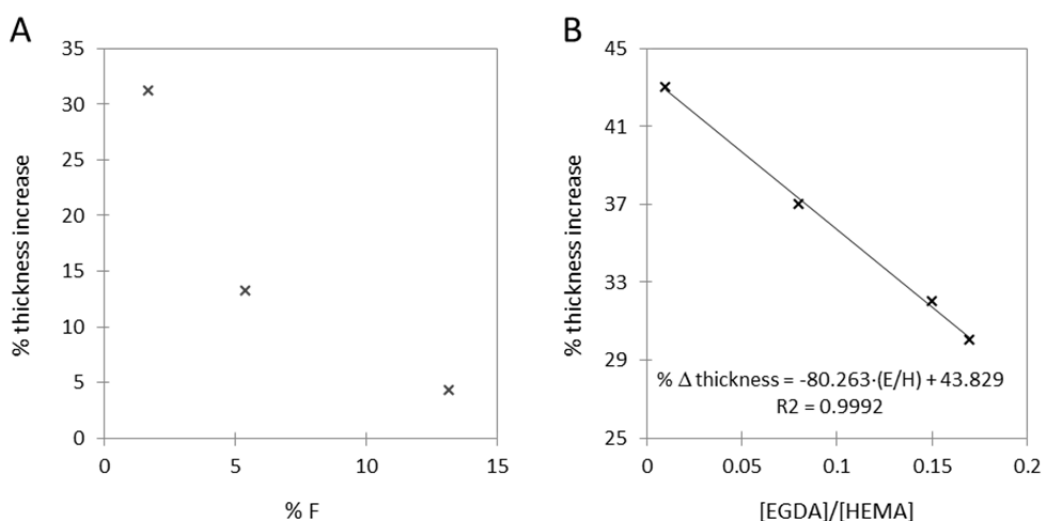


Figure 2.4.3-9. Swelling behavior of the two-layer hydrogels and the bare HEMA-co-EGDA. (A) Thickness increase percentage for three HEMA-co-EGDA / PFM films, maintaining nearly the same degree of crosslinking as function of the amount of fluorine on the surface (XPS). (B) Linear regression of the thickness increase percentage of the HEMA-co-EGDA copolymers versus the EGDA / HEMA ratio.

In view of the final application, the restriction of the swelling ability caused by the PFM was not desirable, since a maximum range in the thickness increase is pursued. However, the subsequent functionalization of the PFM could affect the properties of the film in water, as the interface will change completely. Consequently, it was decided to study the reactivity of the two-layer hydrogels with a more hydrophilic aminated molecule: 2-(2-aminoethoxy)ethanol. The reaction was performed at a concentration of 100 mM in ethanol during 12 h at 37 °C. The two-layer polymer sample before

functionalization had a thickness increase in water as low as 4 % with an EGDA / HEMA of 0.17. After the reaction, the FTIR analysis of the resulting sample showed no C-F stretching peak and the contact angle was reduced from 84° to 67°. Regarding the XPS measurements, the F percentage decreased from 13.19 % to 1.71 %, whereas N increased up to a 0.5 %. Finally, the swelling degree rose from the aforementioned 4 % to a 31 %, which is the thickness increase underwent by a bare hydrogel with the same crosslink density (30 %). Therefore, the samples seemed to be able to recover the intrinsic ability of the hydrogels to swell, once nearly all the PFM had been removed. However, more experiments should be performed to ensure that this effect is not due to a partial coating dissolution.

Dynamic studies of the thickness variation in aqueous media reveal that both hydrogels with and without PFM swelled up to their maximum thickness within the first minute of soaking the sample in water (Figure 2.4.3-10). This indicated that the equilibrium state was quickly reached, regardless of the presence of the fluorinated groups.

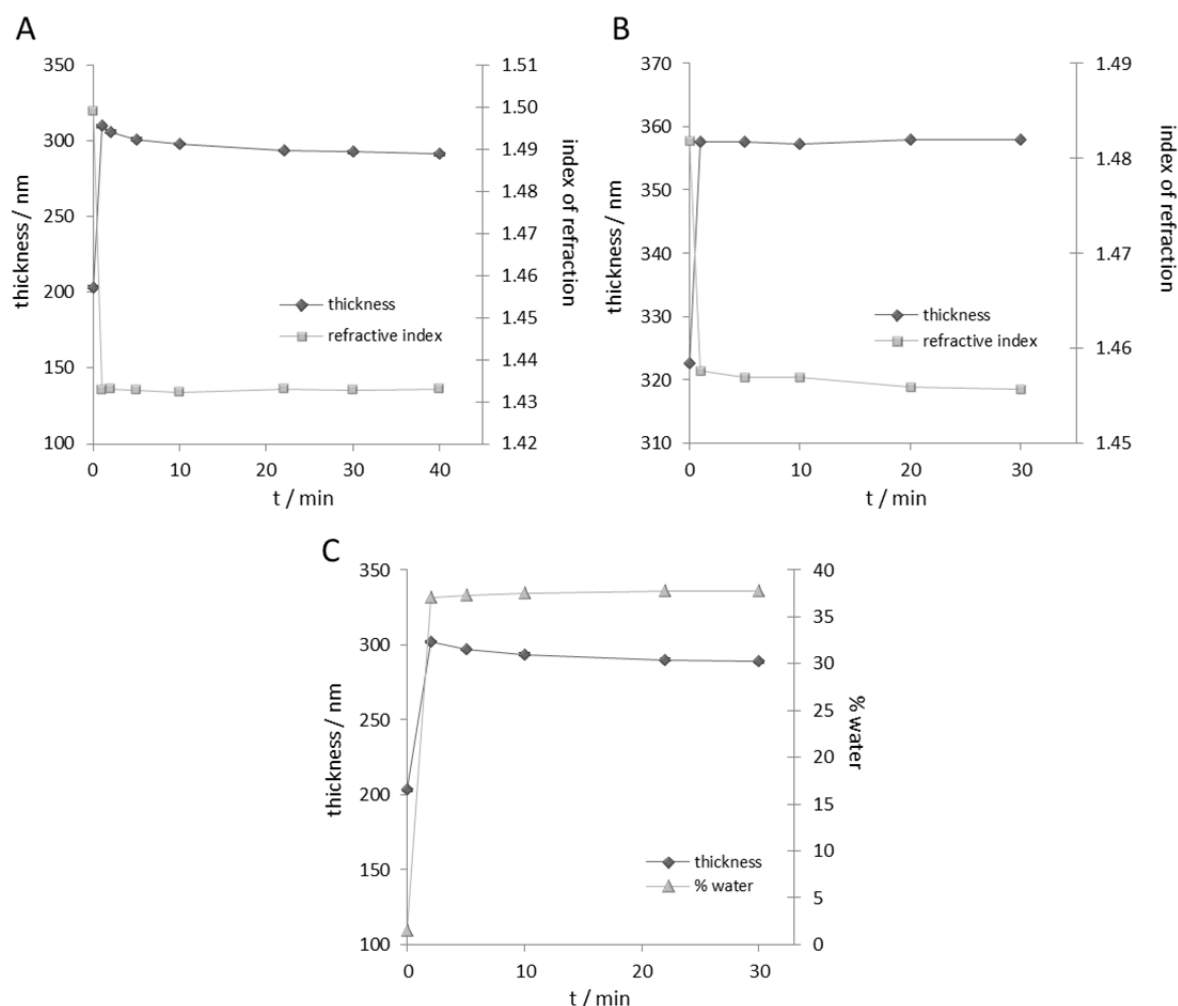


Figure 2.4.3-10. Dynamic swelling studies. Thickness and index of refraction as function of time for (A) a HEMA-co-EGDA copolymer and with an EGDA / HEMA ratio of 0.01 (B) for a two-layer hydrogel (HEMA-co-EGDA / PFM) with an EGDA / HEMA ratio of 0.04. (C) Thickness and water content as function of time for a HEMA-co-EGDA copolymer with an EGDA / HEMA ratio of 0.01.

Figure 2.4.3-10 depicts the thickness of the hydrogels, their refractive index and the percentage of water uptake as function of time for different polymers. Plot A and B correspond to a bare hydrogel and a hydrogel with PFM, respectively. Both presented practically the same profile, as they reached the equilibrium quickly and afterwards maintained their thicknesses. In the case of the hydrogel without PFM, the plateau zone points out a slight decrease of the thickness with time that it was probably due to the partial dissolution of the film, which has a very low crosslinking density. Anyway, the effect is not very significant. As thickness increased, the index of refraction of the samples decreased as expected for the water uptake. Hydrogels with PFM layer always presented higher refractive index, since they incorporated less water. Furthermore, the water content could be predicted using the effective medium approximation (EMA) for the hydrogels without PFM. In the double-layered hydrogels, the films were too complex to obtain a good adjustment. As shown in Figure 2.4.3-10 C, the water content is about 38 % for a HEMA-co-EGDA copolymer with EGDA / HEMA ratio of 0.01 and a thickness increase of 43 %.

Finally, in order to conclude the characterization of the 2-layer films, an analysis of the topography of some of the samples was performed by atomic force microscopy (AFM). The samples were studied in their dry state and also in water to see if there were significant morphological changes.

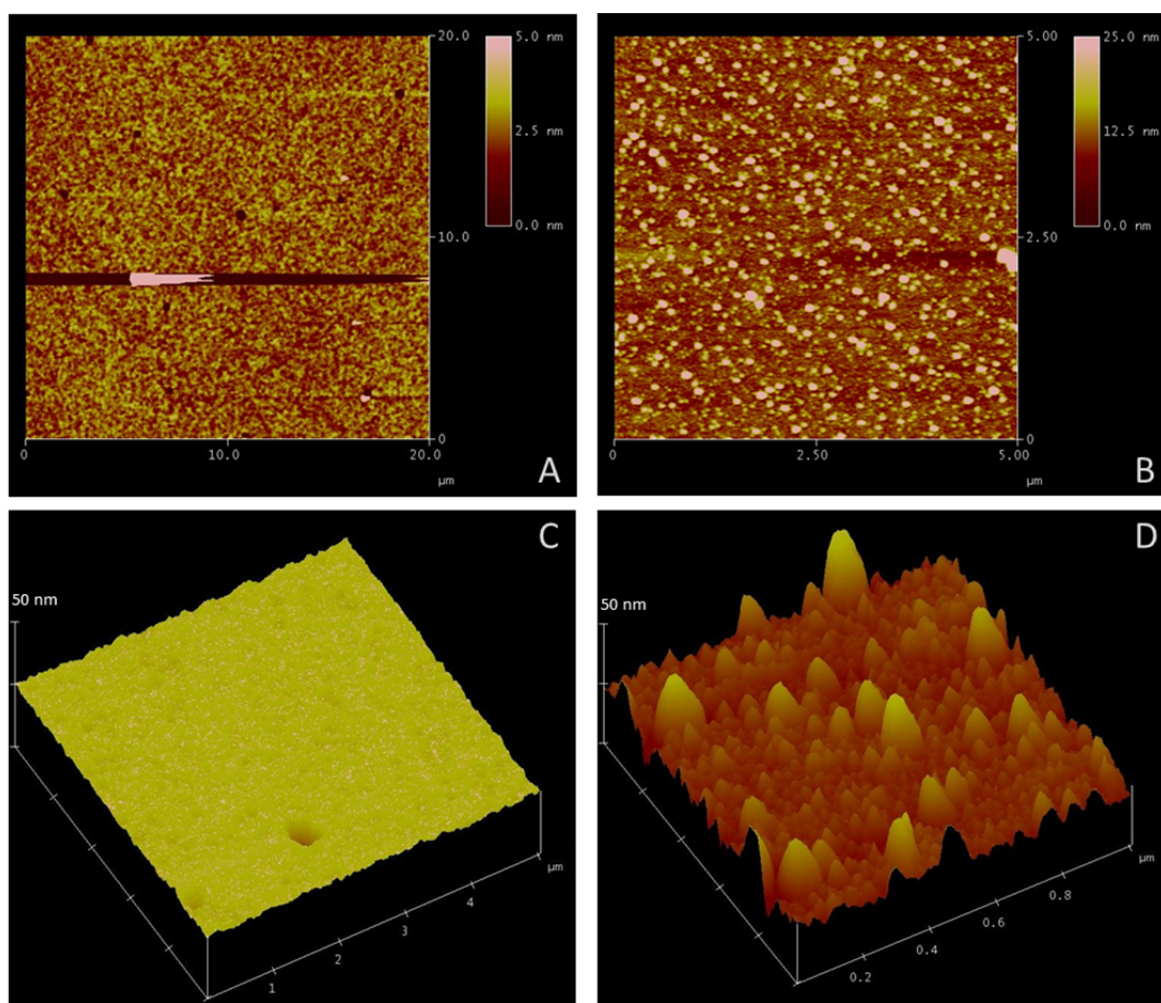


Figure 2.4.3-11. AFM topographical micrographs of a hydrogel with a PFM layer on top. Two-dimensional views of (A) dry sample and (B) in water. Three-dimensional views at the same z-scale (25 nm/division) of (C) dry sample and (D) in water.